Diversification of neuropil organization in specialized and broadly tuned olfactory glomerular circuits in *Drosophila melanogaster*

Lydia Gruber[1], Rafael Cantera[2], Markus William Pleijzier[3], Bill S. Hansson[1#], Jürgen Rybak [1#]

1 Max Planck Institute for Chemical Ecology, Department of Evolutionary Neuroethology, 07745 Jena, Germany
2 Instituto de Investigaciones Biológicas Clemente Estable, Departamento de Biología del Neurodesarrollo, 11600 Montevideo, Uruguay
3 Neurobiology Division, MRC Laboratory of Molecular Biology, Cambridge, CB2 0QH, England, United Kingdom

# contributed equally

*Correspondence: Jürgen Rybak, jrybak@ice.mpg.de

Keywords: olfactory circuitry, DA2, DL5, connectome, *Drosophila melanogaster*, FIB-SEM, synapses, sensory lateralization

ABSTRACT

To manage the great complexity of detecting and identifying olfactory cues, the insect olfactory system has evolved two main strategies: combinatorial coding and specialized, narrowly tuned olfactory pathways. In combinatorial coding, odorants are encoded by activation of multiple, broadly tuned olfactory sensory neurons that innervate distinct sets of glomeruli. In specialized olfactory pathways, information regarding a single or a few odorants is processed in a discrete, narrowly tuned circuit within a dedicated glomerulus. Here, we compared the narrowly tuned glomerulus DA2 with the broadly tuned glomerulus DL5 at the ultrastructural level, by using volume based focused ion beam scanning electron microscopy. We provide a detailed analysis of neuronal innervation, synaptic composition as well as a circuit diagram of the major glomerular cell types: olfactory sensory neurons (OSNs), uniglomerular projection neurons (uPNs) and multiglomerular neurons (MGNs). By comparing our data with a previously mapped narrowly tuned glomerulus (VA1v), we disclose putative generic features of narrowly tuned glomerular circuits: a high density of neuronal fibers and synapses, a low degree of sensory lateralization, strong axo-axonic connections between OSNs as well as dendro-dendritic connections between uPNs, and a low degree of presynaptic inhibition at the OSN axons. We also show a unique property of the large uPN dendrite in DL5, which forms substantial amount of autapses.

INTRODUCTION

Olfaction is an anatomically shallow sensory system. In mammals and invertebrates just one synapse separates the sensory periphery from the central brain (Su et al., 2009;Liang and Luo, 2010;Shepherd, 2011;Owald and Waddell, 2015;Dolan et al., 2018). In the olfactory system of *Drosophila melanogaster*, the first relay station of synaptic transmission is the antennal lobe (AL) which has a circuit architecture homologous to that of the vertebrate olfactory bulb (Boeckh et al., 1990;Sachse and Manzini, 2021;Shepherd et al., 2021). The fly AL consists of approximately 58 spherical compartments, called glomeruli, which can be distinguished by size, shape and location (Laissue et al., 1999;Gao et al., 2000;Vosshall et al., 2000;Grabe et al., 2015;Bates et al., 2020). Each glomerulus receives stereotypic input from axon terminals of olfactory sensory neurons (OSNs), which have their cell bodies and dendrites located in the antennae or maxillary palps (de Bruyne et al., 1999;Shanbhag et al., 1999;de Bruyne et al., 2001;Hallem et al., 2004;Benton et al., 2006). All the OSNs innervating a given glomerulus express a typical repertoire of ligand-gated chemoreceptors (Couto et al., 2005;Fishilevich and Vosshall, 2005;Benton et al., 2006), which represent a wide range of specifications, binding either a single, few, or many distinct chemicals (Hallem et al., 2004;Hallem and Carlson, 2006;Knaden et al., 2012;Münch and Galizia, 2016;Seki et al., 2017;Wicher and Miazzi, 2021).

Most OSNs project bilaterally to the corresponding glomeruli in the left and right AL (Gaudry et al., 2013;Tobin et al., 2017). In the AL, OSNs convey odor signals to excitatory uniglomerular projection neurons (uPNs), which branch only within a single glomerulus, or to inhibitory multiglomerular PNs (mPNs) and (inhibitory or excitatory) interglomerular local interneurons (LNs) (Ng et al., 2002;Cuntz et al., 2007;Kazama and Wilson, 2008;Kreher et al., 2008;Kazama and Wilson, 2009;Masse et al., 2009;Tanaka et al., 2012;Ai and Hagio, 2013;Wilson, 2013;Bates et al., 2020). LNs innervate several glomeruli and are the key modulatory neurons in the AL (Chou et al., 2010;Seki et al., 2010). The highly converging OSNs-to-PN signal transmission (Chen and Shepherd, 2005;Masse et al., 2009;Jeanne and Wilson, 2015) is lateralized, activating ipsilateral uPNs more strongly than contralateral ones (Agarwal and Isacoff, 2011;Gaudry et al., 2013;Tobin et al., 2017). From the AL, uPNs and mPNs relay processed signal information to higher brain centers (Norgate et al., 2006;Fiala, 2007;Jefferis et al., 2007;Keene and Waddell, 2007;Galizia, 2014;Guven-Ozkan and Davis, 2014;Strutz et al., 2014;Bates et al., 2020).

The stereotypic activity pattern of the olfactory glomeruli by distinct odorants encodes the odor space, represented in a so-called odotopic map of the AL according to the glomerular activation by distinct chemical classes. (Couto et al., 2005;Laissue and Vosshall, 2008;Knaden and Hansson, 2014;Grabe et al., 2015;Grabe and Sachse, 2018). Some odorants induce a fixed innate behavior (aversion or attraction), activating characteristically specific glomeruli (Semmelhack and Wang, 2009;Knaden et al., 2012;Knaden and Hansson, 2014;Gao et al., 2015;Grabe and Sachse, 2018). The encoding of hedonic valence already at the level of the AL is important for a fast odor

coding. Most odorants are encoded in a combinatorial manner in the fly AL by activating multiple OSNs types expressing broadly tuned receptors and their glomerular circuits, including broadly tuned uPNs (de Bruyne et al., 2001;Silbering and Galizia, 2007;Silbering et al., 2008;Masse et al., 2009;Galizia, 2014;Szyszka and Galizia, 2015;Sachse and Hansson, 2016;Seki et al., 2017). Certain chemoreceptors and their downstream glomerular circuit, however, have evolved a very high specificity and sensitivity to single or very few chemicals (Andersson et al., 2015;Haverkamp et al., 2018;Keesey and Hansson, 2021). These narrowly tuned glomerular circuits often belong to dedicated olfactory pathways, called "labeled lines", which process information regarding single odorants of particular importance for reproduction and survival (Kurtovic et al., 2007;Datta et al., 2008;Stensmyr et al., 2012;Dweck et al., 2015;Gao et al., 2015). An extreme example is the DA2 glomerulus, which responds exclusively to geosmin, an ecologically relevant chemical that alerts flies to the presence of harmful microbes, causing the fly to avoid laying eggs at these locations (Stensmyr et al., 2012). This dedicated olfactory pathway and its receptor sequence is conserved throughout evolution (Keesey et al., 2019;Keesey and Hansson, 2021). Another example is glomerulus VA1v, which responds to methyl laurate, a pheromone that induces a strongly attractive response in female flies leading to aggregation behavior (Dweck et al., 2015). DL5, on the other hand, is an example of a broadly tuned glomerulus, innervated by OSNs activated by several aversive odorants, like E2-hexenal or benzaldehyde (Knaden et al., 2012;Münch and Galizia, 2016;Seki et al., 2017;Mohamed et al., 2019b). This functional diversity suggests differences in neuronal composition and synaptic connectivity between broadly and narrowly tuned glomeruli.

A survey of neuronal composition across glomeruli revealed great variation in the numbers of the different types of neurons innervating narrowly and broadly tuned glomeruli (Grabe et al., 2016). In general, narrowly tuned glomeruli were found to be innervated by more uPNs and fewer LNs compared to more broadly tuned glomeruli (Chou et al., 2010;Grabe et al., 2016). In addition, narrowly tuned OSNs received less global interglomerular LN inhibition than broadly tuned ones (Hong and Wilson, 2015;Grabe et al., 2020;Schlegel et al., 2021). For example, in female flies, the narrowly tuned glomerulus DA2 contains dendrites of 6-8 uPNs, whereas the broadly tuned glomerulus DL5 houses only 1 or 2 uPNs and has a higher number of innervating LNs. Interestingly, both glomeruli are innervated by the same number of OSNs (Grabe et al., 2016).

Little is known, however, about the microarchitecture of the synaptic circuitry in distinct glomeruli and, in particular, about principal ultrastructural differences between narrowly vs. broadly tuned glomerular circuits. Electron microscopy (EM) allows volume imaging with dense reconstruction of fine neurite branches and synapses in brain tissue at nanometer resolution, necessary to map synapses (Briggman and Denk, 2006;Cardona et al., 2009;Helmstaedter, 2013;Rybak, 2013;Meinertzhagen, 2018). The first ultrastructural insights into the synaptic connectivity of *Drosophila* olfactory glomeruli were obtained by studies based on serial

124 section transmission EM (ssTEM) (Rybak, 2016;Tobin et al., 2017). In these studies,
125 Rybak *et al*. (2016) showed that all 3 basic classes of AL neurons make synapses with
126 each other, while Tobin *et al*. (2017) revealed that the differences in number of
127 innervating uPNs between the left and right DM6 glomeruli are compensated by
128 differences in synaptic strength. With focused ion beam-scanning electron microscopy
129 (FIB-SEM; (Knott et al., 2008)) a complete reconstruction of all neurons in the narrowly
130 tuned, pheromone processing glomerulus VA1v was obtained (Horne et al., 2018).
131 Recent technological innovations in ssTEM, FIB-SEM and automated neuron
132 reconstruction have made connectome datasets of the adult *Drosophila* central nervous
133 system available (Saalfeld et al., 2009;Zheng et al., 2018;Li et al., 2020b;Scheffer et al.,
134 2020) and provided complete circuit descriptions of several brain centres (Felsenberg
135 et al., 2018;Dolan et al., 2019;Auer et al., 2020;Bates et al., 2020;Coates et al.,
136 2020;Huoviala et al., 2020;Li et al., 2020a;Marin et al., 2020;Otto et al., 2020;Hulse et al.,
137 2021;Schlegel et al., 2021).
138 In an attempt to find answers to how highly specialized olfactory glomerular
139 circuits of dedicated olfactory pathways differ in their signal integration from broadly
140 tuned glomerular circuits, we compared the microarchitecture and synaptic circuitry
141 of a narrowly and a broadly tuned glomerulus (DA2 and DL5). By using a correlative
142 workflow combining transgenic markers with FIB-SEM, in order to identify our
143 glomeruli of interest, we reconstructed OSNs, uPNs and multiglomerular neurons
144 (MGNs) and mapped all associated synapses and compared the circuit organization
145 of both glomeruli.
146

147 **RESULTS**

148 ## Volume-based electron microscopy of two different olfactory glomeruli

149 To compare the synaptic circuitries of two olfactory glomeruli known to belong
150 to either narrowly or broadly tuned glomerular types in *Drosophila melanogaster*, we
151 mapped all synapses of glomeruli DA2 (right AL) and DL5 (left AL) in one female fly
152 (**Figure 1A-B**) with the aid of focused ion beam scanning electron microscopy (FIB-
153 SEM). A partial reconstruction of a second DA2 in another fly was used for neuronal
154 volume measurements (see Methods). The reconstructions were based on high
155 resolution (4x4x20 nm) datasets (**Figure 1**; **Figure 1 – video 1),** thus allowing
156 reconstruction of fine neuronal branches (~20 nm diameter; **Figure 1C-D**) as well as
157 mapping chemical synapses (example in **Figure 1E**) in the two volumes of interest
158 (VOI). To restrict the imaging volume to the target VOIs, we employed a correlative
159 approach for the first time for a *Drosophila* EM volume reconstruction. The glomeruli
160 of interest were identified by their size, shape and location in brains of transgenic flies
161 (*Orco-GAL4; UAS-GCaMP6s*) using the glomerular map of (Grabe et al., 2015). The flies
162 expressed the protein GCaMP6, a green fluorescent protein coupled with calmodulin
163 and M13 (a peptide sequence from myosin light-chain kinase; **Figure 1A-B**).
164 Subsequently, the identified glomeruli were marked by laser branding using a two-
165 photon laser (Bishop et al., 2011). These fiducial marks were apparent under both light
166 (Figure 1A-B) and electron microscopy **(Figure 1C-D)** and facilitated the delimitation
167 of the VOIs during FIB-SEM scanning. We produced two complete FIB-SEM datasets:
168 one for glomerulus DA2 and one for DL5 (pure imaging time for both glomeruli: ~60
169 h) and a partial dataset for DA2 in a second fly.
170

171 ## Skeleton based neuron reconstruction and synapse identification

172 We reconstructed all neurons within the two VOIs (example neuron: **Figure 1F**)
173 and mapped all their synaptic connections using an iterative skeleton-based
174 reconstruction approach, similar to previously reported procedures (Berck et al.,
175 2016;Schneider-Mizell et al., 2016;Zheng et al., 2017) with the aid of the web-based
176 neuron reconstruction software CATMAID (http://www.catmaid.org;
177 RRID:SCR_006278; (Cardona et al., 2009;Schneider-Mizell et al., 2016); **Figure 1 –**
178 **video 1**). Synapses were identified by their presynaptic transmitter release site, which
179 in *Drosophila* is composed of a presynaptic density called a T-bar, surrounded by
180 synaptic vesicles and apposed postsynaptic elements (**Figure 1E**), as previously
181 described (Trujillo-Cenoz, 1969;Fröhlich, 1985;Rybak et al., 2016;Huang et al., 2018;Li
182 et al., 2020b). All synapses observed in our FIB-SEM data sets were polyadic, i.e. each
183 presynaptic site connected to multiple postsynaptic sites (See example in **Figure 1E**),
184 a feature of insect brain synapses (Meinertzhagen and O'Neil, 1991;Malun et al.,
185 1993;Prokop and Meinertzhagen, 2006;Hartenstein, 2016;Rybak et al., 2016). Some
186 synaptic complexes had up to 16 postsynaptic sites (**Figure 2 – figure supplement 1B**),

187 i.e. one T-bar to 16 single synaptic profiles (i.e. 1:1 single output-input connections).
188 Short neuronal fragments (<10 µm), which could not be connected to any neuronal
189 fiber were designated as "orphans". These fragments represented 4% of the total
190 length of all traced neuronal fibers in DA2 and 6% in DL5 and contained about ~12%
191 of all synaptic contacts in both glomeruli.
192

193 **Glomerular neurons: classification, description and inventory**

194 Previous descriptions of the ultrastructural characteristics of the AL in *Drosophila*
195 helped to classify AL neurons into 3 main classes (**Figure 2A**) Olfactory sensory
196 neurons (OSNs), uniglomerular projection neurons (uPNs) and multiglomerular
197 neurons (MGNs; cells that interconnect multiple glomeruli). MGNs are further
198 subdivided into multiglomerular projection neurons (mPNs) and local interneurons
199 (LNs) (Berck et al., 2016;Rybak et al., 2016;Zheng et al., 2017;Gruber et al., 2018;Horne
200 et al., 2018;Li et al., 2020b;Schlegel et al., 2021). Most of the neuronal profiles within
201 the MGN neuron class are probably inhibitory local neurons, as this cell type is the
202 most numerous and broadly arborizing of the multiglomerular cell types in the
203 antennal lobe (Chou et al., 2010;Lin et al., 2012). In addition, we observed a few
204 neuronal fibers with an electron-dense and vesicle-rich cytosol, which we interpreted
205 to be either peptidergic neurons (Nässel and Homberg, 2006;Eckstein et al., 2020) or
206 the contralaterally projecting, serotonin-immunoreactive deutocerebral (CSD)
207 neuron, (Dacks et al., 2006;Goyal and Chaudhury, 2013;Zheng et al., 2017;Coates et al.,
208 2020;Eckstein et al., 2020). Except for these neuronal fibers containing abundant
209 electron-dense vesicles, all other neuronal fibers were assigned to either OSNs, uPNs
210 or MGNs based on their morphologies (**Figure 2A, B;** see Methods).
211 OSNs formed large, elongated synaptic boutons (**Figure 2A**), had the largest
212 volume/length ratio of all three neuron classes (**Figure 2 – figure supplement 1A**) and
213 displayed the lowest degree of branching intensity of all neurons in both glomeruli
214 (**Figure 2B**). In agreement with what had been observed in other glomeruli (Rybak et
215 al., 2016), the majority of output synapses made by OSN terminals were triads (1:3)
216 and tetrads (1:4). The T-bars of OSN synapses exhibited a large variation in length:
217 some were large enough to accommodate 16 postsynaptic contacts (**Figure 2 – figure**
218 **supplement 1B).** The frequency of large T-bars was much higher in OSNs than in
219 other neuron classes with an average polyadicity (average number of postsynaptic
220 sites at each T-bar) of 6 (1:6; (**Table 1,** row 14). As OSNs had the greatest T-bar and
221 output density along their axons (**Table 1**, row 10-11) they also displayed the largest
222 synaptic ratios (both for the T-bars/input sites and output sites/input sites) of all
223 neuron classes (**Table 1,** row 12-13), which was in line with previous observations
224 (Rybak et al., 2016).
225 The uPNs exhibited the highest degree of branching intensity of the three neuron
226 classes in both glomeruli (**Figure 2A-B**). They showed numerous very fine apical
227 branches that frequently connected multiple times via spines to the same presynaptic
228 site, leading to an entangled 3D shape typical of uPNs (**Figure 2A**) (Rybak et al.,

229 2016;Tobin et al., 2017;Schlegel et al., 2021). uPNs had the smallest volume/length ratio
230 of all neuron classes (for the DA2: **Figure 2 - supplement 1A**). In addition to having
231 many fine branches, uPN dendrites also had enlarged regions with almost no cytosol
232 that were packed with large mitochondrial profiles extending over considerable
233 distances. These enlarged profiles showed a larger degree of mitochondria fission
234 (dividing and segregating mitochondrion organelles; personal observation) than the
235 other neuron classes with rather round and compact mitochondria (**Figure 2A**; FIB-
236 SEM image; see data availability). In glomerulus DA2 we found 7 uPNs, consistent
237 with previous reports (Grabe et al., 2016). Two of them (PN#1, PN#2; see data
238 availability) branched broadly and innervated the full glomerulus, receiving more
239 synaptic input than the other 5 uPNs (PN#3-#7; **see Table S3**), which branched
240 exclusively in sub-regions of the glomerulus, with partial overlap. In addition to
241 abundant clear small vesicles (~20 nm in diameter) (Yasuyama et al., 2003;Strutz et al.,
242 2014;Bates et al., 2020), uPN dendrites also displayed small electron-dense vesicles, as
243 previously reported for PN axon terminals in the mushroom body calyx (Butcher et
244 al., 2012;Yang et al., 2022). These electron-dense vesicles are packed with different
245 types of neuropeptides that act as neuromodulators or co-transmitters (Gondré-Lewis
246 et al., 2012;Li et al., 2017;Croset et al., 2018;Eckstein et al., 2020). In both glomeruli,
247 uPNs had the highest neuronal synaptic input density and the lowest T-bar and
248 output density of the three neuron classes (**Table 1,** row 9-11; DA2 and DL5
249 differences: see next section). The synaptic ratios (T-bars/input sites and output
250 sites/input sites) were much lower for uPNs than for the other neuron classes (**Table**
251 **1,** row 12-13). The majority of uPN dendritic output synapses (feedback synapses)
252 were tetrads in both glomeruli, with an average polyadicity of around 5 (lower than
253 in OSNs; (**Figure 2 – supplement 1; Table 1,** row 14).
254 The majority of the neuronal fibers in both glomeruli belonged to MGNs (**Figure**
255 **2A**). MGNs exhibited variable morphology and ultrastructure, as expected, but shared
256 also some ultrastructural features. Their synaptic boutons were formed by thin fibers,
257 thus the volume/length ratio of MGNs was lower than that of OSNs but greater than
258 that of uPNs (**Figure 2 – figure supplement 1A**). A similar relationship was found for
259 the number of output sites and the T-bar density along MGN fibers, which were
260 smaller than in OSNs but larger than in uPNs (**Table 1,** row 10-11). In contrast,
261 branching intensity in MGNs was larger than in OSNs but smaller than in uPNs
262 (**Figure 2B**). The synaptic ratio of output-to-input sites was around one (**Table 1**, row
263 12-13). MGNs had the lowest polyadicity (~3) of the three neuron classes (**Table 1**, row
264 14) and their synapses were mainly triads (**Figure 2 – supplement 1D**). Interestingly,
265 besides the abundant clear small vesicles (~20 nm in diameter), some MGNs had small
266 electron-dense vesicles, most likely housing the neuropeptide sNPF (Nässel et al.,
267 2008).
268
269 **DA2 is more densely innervated and has a higher synapse density than DL5**

In our FIB-SEM datasets the volume of glomerulus DA2 was 45% smaller than that of glomerulus DL5 (1500 μm^3 vs. 2700 μm^3), which is in agreement with measurements based on light microscopy (DA2 = 1600 μm^3, DL5 = 2900 μm^3 (Grabe et al., 2016). We also confirmed that a similar number of OSNs (44-46 OSNs) innervated both glomeruli (**Figure 2C**), and that each glomerulus received OSN innervation from both the ipsilateral and contralateral antennae (Vosshall et al., 2000;Grabe et al., 2016). Also in agreement with (Grabe et al., 2016), the DA2 glomerulus was innervated by 7 uPNs whereas DL5 had a single uPN (**Figure 2C**). MGN cell numbers could not be counted in our study due to their multiglomerular morphology, which also prevented us from tracing MGN fibers to their soma due to our partial volume acquisition (see Methods).

To further investigate differences in neuronal populations we now turned our attention to the glomerular innervation and synaptic composition of DA2 and DL5 neuronal fibers (Grabe et al., 2016). We measured the total length (sum in µm) of all neuronal fibers of each neuron class within the DA2 and DL5 (**Figure 2C; Table 1**, row 1). In addition, we counted all T-bars and their output sites (1:1 synaptic contacts) as well as all postsynaptic sites (input sites) for all neuron fibers together and of each neuron class individually (**Table 1, row 2-4**). We counted in total ~ 14 000 synaptic contacts and 2648 T-bars in DA2 and ~ 17 000 contacts and 3387 T-bars in DL5 (**Figure 2C, Table 1, row 4**). Most of these synapses were triads and tetrads (**Figure 2 – figure supplement 1B-D**). In order to compare DA2 and DL5 we normalized neuronal length and synaptic counts to glomerular volume. We then analyzed (**1**) the innervation density, i.e., the length of neurons per glomerular volume ($\mu m/\mu m^3$) and (**2**) the glomerular synaptic density (T-bar #, output site or input site #/μm^3). Data are reported in total for all neuronal fibers of each neuron class (**Table 1, row 5-8**) and as an average for neuronal fibers of the respective neuron class **(Figure 3)**. In addition, we compared (**3**) the average polyadicity for each neuron class **(Figure 3)** and **(4)** the average neuronal synaptic density (T-bar, output and input site density along each neuronal fiber) (#/µm) (**Figure 3 – figure supplement 1B**).

We observed that the average neuron innervation density of OSNs was significantly higher in DA2 than in DL5, with a total innervation density that was 20% higher in DA2 (**Figure 3A**), **Table S1**). The glomerular synaptic density of input sites, output sites and T-bars along OSNs was significantly higher in DA2 than in DL5 (**Figure 3A**). OSNs in DA2 formed therefore more input sites, and much more T-bars and output sites per glomerular volume than in DL5 (**Table 1**, row 7-8; relative differences: **Table S1**). In contrast, the density of input sites distributed along the length of OSN fibers was similar in DA2 and DL5, whereas T-bar and output site density along the OSN axons was significantly higher in DA2 (**Figure 3 – figure supplement 1A**).

We then asked if the DA2 glomerulus, due to its higher number of uPNs, also had a higher uPN innervation density and synaptic density of its postsynaptic sites and/or presynaptic sites compared to the DL5 glomerulus, which contains a single uPN. In the DA2, the fibers of the 7 uPNs had almost the same total length as the fibers

313 of the single uPN in the more voluminous DL5 (4652 μm in DA2 vs. 5015 μm in DL5;
314 **Table 1**, row 1). The DA2 uPNs had in addition a similar total number of input sites
315 as the single uPN in the DL5 (3887 vs. 3955; **Table 1**, row 2). As such, in DA2 the total
316 innervation density of its 7 uPNs was higher as compared to the innervation density
317 of the single uPN in DL5 (**Table 1**, row 5), even though the average innervation
318 density of DA2-uPNs was lower (**Figure 3B**). The total glomerular input density of all
319 uPNs was higher in DA2 as compared to DL5 (**Table 1**, row 6). On the other hand, the
320 total glomerular synaptic density of the T-bars and output sites was similar in DA2
321 and DL5 (**Table 1**, rows 7-8). In line with these results, the neuronal density of T-bars
322 and output sites was less in the DA2 uPNs as compared to the DL5 uPN, whereas the
323 neuronal density of input sites was similar (**Figure 3 – figure supplement 1B; Table**
324 **1**, row 9-10). This caused almost twice as high synaptic ratios (T-bars-to-inputs and
325 outputs-to-inputs) in the DL5 uPN relative to DA2 uPNs (**Table 1**; row 12-13).
326 We then hypothesized that DA2 will have a lower innervation density of MGNs
327 (mainly LNs) than DL5 as it had been reported that DL5 is innervated by fewer LNs
328 (Chou et al., 2010;Grabe et al., 2016). However, we observed the opposite: the
329 innervation density of MGNs was significantly higher in DA2 than in DL5 (**Figure**
330 **3C**), with slightly higher total innervation density (**Table 1,** row 5**).** Interestingly, only
331 the glomerular input density was significantly higher for DA2 MGNs compared to
332 that found in DL5, not the glomerular synaptic density of output sites or of the T-bars
333 (**Figure 3C**). However, the total glomerular synaptic density of input sites, output sites
334 and T-bars were still higher in DA2 than in DL5 **(Table 1,** rows 6-8**).** Synaptic densities
335 along the MGN fibers were similar in DA2 and DL5 (**Figure 3 – supplement 1**).
336 In summary, the DA2 glomerulus is more densely innervated than DL5 with
337 neuronal fibers, which results in a more densely packed DA2 neuropil with more
338 synaptic contacts. The DA2 has a significantly higher innervation density and higher
339 density of T-bars, output and input sites per volume (**Figure 3D**, **Table 1,** row 5-8**).**
340 The degree of synapse polyadicity is also significantly higher in DA2 than in DL5
341 (**Figure 3D, Table 1,** row 14) due to a shift to higher polyadicity among OSN (**Figure**
342 **3A**) and MGN synapses (**Figure 3C**). OSNs show the strongest shift in polyadicity,
343 with tetrads being the most abundant synapse type in DA2 whereas triads are the
344 most abundant in DL5 OSNs (**Figure 2 – figure supplement 1B).**
345

346 ## Lateralization of OSN glomerular connectivity

347 In *Drosophila melanogaster*, the majority of olfactory glomeruli receive bilateral
348 OSN input (Stocker et al., 1983;Stocker et al., 1990;Vosshall et al., 2000;Silbering et al.,
349 2011) see scheme in **Figure 4A**). Recent studies have shown that ipsi- and contralateral
350 OSNs are asymmetric in their synaptic connectivity to other neurons in the majority
351 of the glomeruli (Tobin et al., 2017;Schlegel et al., 2021) and that ipsi- and contralateral
352 OSNs activate uPNs in an asymmetric way (Gaudry et al., 2013;Tobin et al., 2017).
353 However, not all glomeruli appear to have the same degree of lateralized OSN
354 connectivity (Schlegel et al., 2021). At least for one narrowly tuned glomerulus (DA1),

355 there is functional evidence that in female flies its uPNs are evenly activated by either
356 ipsi- or contralateral antennal stimulation (Agarwal and Isacoff, 2011). We
357 hypothesized that this lack of lateralization could be a feature of other narrowly tuned
358 glomeruli.
359 Ipsi- and contralateral OSNs in DA2 and DL5 were identified based on the
360 location and trajectory of their axons (**Figure 4B**). In both glomeruli, ipsilateral OSN
361 terminals were longer than their contralateral counterparts within the VOI, while
362 polyadicity was stronger in contralateral axons. Synaptic density was not consistently
363 higher or lower in ipsilateral OSNs compared to contralateral ones in DA2 and DL5
364 (**Figure 4 – figure supplement 1**).
365 We observed that the synaptic output of ipsi- vs. contralateral OSNs was
366 asymmetric, with significant differences in the ipsi- and contralateral OSN output to
367 either uPNs, OSNs or MGNs (**Figure 4C**, DA2 and DL5). In agreement with previous
368 observations in other glomeruli (Schlegel et al., 2021), the output fraction to uPNs and
369 OSNs was greater in ipsilateral OSNs than in contralateral ones (**Figure 4C**, DA2 and
370 DL5). Vice versa, the OSN output to MGNs was greater in the contralateral
371 glomerulus than the ipsilateral side (**Figure 4C**, DA2 and DL5). However, the
372 differences between the medians and means were smaller in DA2 than in DL5 (**Figure**
373 **4C**; differences between means: see data availability).
374 Our finding of less lateralized connections in the DA2 (**Figure 4C**, DA2 and DL5)
375 was also observed in another narrowly tuned glomerulus (VA1v; Dweck et al., 2015)
376 for which connectome data is available (Horne et al., 2018). In VA1v, the OSN output
377 to uPNs and MGNs was significantly asymmetric in the same manner as in DA2 and
378 DL5, i.e. with greater ipsilateral OSN output fractions to uPNs and OSNs and greater
379 contralateral OSN output fraction to MGNs (**Figure 4C**). Asymmetry in the VA1v OSN
380 output fractions was even less distinct than in DA2 (regarding both the difference
381 between the median and the mean; **Figure 4C** and data availability). In VA1v, the OSN
382 output fraction to OSNs was similar in ipsi- and contralateral OSNs (**Figure 4C**). In
383 addition, the OSN input, from either sister OSNs or MGNs, was asymmetric in DL5
384 but not in the narrowly tuned glomeruli (**Figure 4D**). The inputs from uPNs to ipsi-
385 or contralateral OSNs were not compared due to their low numbers.
386 In summary, our data add to the knowledge of lateralized connectivity within
387 olfactory glomeruli and supports the hypothesis that narrowly tuned glomeruli have
388 a lower degree of lateralization of OSN connectivity compared to broadly tuned
389 glomeruli.
390

391 ## Glomeruli DA2 and DL5 differ in several features of their circuitry

392 Next, we asked whether the synaptic circuitries of DA2 and DL5 differ from each
393 other. We counted each synaptic contact (**Table S2 and S3**) and categorized the
394 distinct connection motifs according to the neuron class the output and input neuron
395 belonged to (**Figure 5A; Table S2).** Each connection motif (for example OSN>uPN, i.e.,
396 the OSN-to-uPN feedforward connection) was then assessed for its relative synaptic

strength, i.e. how many synaptic contacts of this particular connection motif were found compared to the total number of synaptic contacts within the respective circuitry (**Figure 5A-D**; see Methods).

We found that neurons from each class made synaptic contacts with each other in DA2 and DL5, as previously reported for other glomeruli (Berck et al., 2016;Rybak et al., 2016;Tobin et al., 2017;Horne et al., 2018;Schlegel et al., 2021). In both DA2 and DL5, OSNs provided the strongest relative synaptic output, i.e. 49% of all synaptic connections in DA2 and 43% in DL5 were formed by OSNs (**Figure 5B-C**). Thus, even though DA2 and DL5 had similar numbers of OSNs (44 and 46, respectively), those in DA2 provided a stronger circuit output (14% stronger; **Table S2**) than those in DL5 (**Figure 5B-C)**. In both glomeruli the main OSN output partners were MGNs and uPNs, i.e. 27% of all circuitry connections in DA2 and 24% in DL5 were OSN>MGN connections and 20% in DA2 and 18% in DL5 were OSN>uPN connections (**Figure 5B-C**). In DA2, interestingly, each of the 7 uPNs received input from almost all OSNs and so could maintain a high degree of convergent signal transmission (**Table S3**). In contrast, OSNs received the lowest relative input of all neuron classes in DA2 and DL5 (7% and 8% respectively; **Figure 5B-C**). In line with previous observations in other glomeruli (Horne et al., 2018;Schlegel et al., 2021), OSNs also made abundant axo-axonic synapses with sister OSNs (2.6% in DA2 and 1.5% in DL5; **Figure 5B-C**). Thus, the relative synaptic strength of the OSN>OSN connection was 70% stronger in DA2 than in DL5 (**Figure 5B-C; Table S2**).

The uPNs in both glomeruli had the weakest relative output of all neuron classes within their circuitry, and this was even weaker (38%) in DA2 (**Figure 5B-C; Table S2**). In contrast, the relative synaptic input onto uPNs was greater in DA2 than in DL5 (33% vs. 28%, respectively; **Figure 5B-C;** 16% stronger in DA2; **Table S2**), which is in line with our finding that in DA2, the uPNs provide more input sites per unit of glomerular volume than in the DL5 (**Figure 3B-C**). In both glomeruli, the feedback connections from uPNs (depicted in **Figure 5A**), were almost exclusively directed towards MGNs, as previously reported for the broadly tuned DM6 and the narrowly tuned glomerulus VA1v (Tobin et al., 2017;Horne et al., 2018). However, the relative synaptic strength of the uPN>MGN connection was 40% weaker in DA2 than in DL5 (uPN>MGN: 10% in DA2 and 17% in DL5). Only a few cases of uPN>OSN synaptic connections were observed (a total of 16 in DA2 and 26 in DL5) representing a synaptic strength of 0.1% in DA2 and 0.2% in DL5 (**Table S2**). Finally, uPNs in DA2 also made 71 reciprocal synaptic connections (representing a synaptic strength of 0.6%; **Table S2**; **Figure 5B**), consistent with electrophysiological evidence for reciprocal synaptic interactions between sister uPNs (Kazama and Wilson, 2009). The single uPN of the DL5 had 54 dendro-dendritic synapses (representing 0.4% of all DL5 synaptic contacts; **Figure 5C**), which were exclusively autapses, i.e. synapses formed by a neuron onto itself. Dendritic uPN autapses exist also in DA2-uPNs, but they were few: we observed only 14 autaptic uPN-uPN connections in DA2, which were mainly located at the two longest uPN dendrites (for further analysis of autapses see next section).

MGNs received the strongest input in both glomeruli (60% of the total input in DA2 and 64% in DL5; **Figure 5B-C**). This is in line with the observation that MGNs provided the majority of all traced neuronal fibers in each glomerulus and had the highest innervation density of all neuron classes; **Table 1**). The relative output strength of MGNs was similar in both glomerular circuits (~40% of the total output in each glomerulus; **Figure 5B-C**). MGNs made many reciprocal synapses to each other, accounting for 23% of all synapses in both glomeruli (**Figure 5B-C)**. The relative synaptic strength between MGN>uPN was stronger in DA2 (12%) than DL5 (10%) (**Figure 5B**-C; **Table S2**). The MGN>OSN feedback connection was relatively weak in both glomeruli (5% in DA2 vs. 6% in DL5; **Figure 5B-C**) but weaker (25%) in DA2 than in DL5 (**Table S2**).

We then looked at the fractional output and input of each neuron class (Figure 5E′, E′′). In both glomeruli OSNs had a similar proportion of their synaptic output onto uPNs (40%-41%), onto MGNs (55% in both) and onto sister OSNs (4%-5%) (**Figure 5E′**). From the uPNs perspective, over 93%-96% of their recurrent synaptic output was directed to MGNs in both DA2 and DL5, and few synapses were directed onto OSNs (~1% of the uPN output; **Figure 5E′**). The uPN>uPN output fraction of the 7 uPNs in DA2 (reciprocal synapses) was twice the uPN output fraction (autaptic) of the single uPN dendrite in DL5 (6% vs. 3%; **Figure 5E′**). MGNs formed synaptic output mainly to other MGNs (58%-59% of the total MGN output in DA2 and DL5). Among MGNs we found also rare cases of autapses. The MGN>uPN output fraction was greater in DA2 (30%) than in DL5 (25%), whereas the MGN>OSN output fraction was smaller in DA2 (12%) than in DL5 (16%; **Figure 5E′**).

Turning to the input fractions of each neuron class, we found that in both glomeruli, OSNs received most of their input from MGNs (>50%). In DA2 the input fraction onto OSNs (MGN>OSN) was smaller than in DL5 (63% vs. 78%; **Figure 5E′′**). In contrast, the OSN input fraction from sister OSNs was greater in DA2 (35% vs. 20%; **Figure 5E′′**). In both glomeruli, the OSNs received only weak uPN input (2%) (**Figure 5E′′**). The input fractions onto the 7 uPNs, formed by uPNs, MGNs and OSNs, in the DA2 and the single uPN in DL5 were similar (**Figure 5E′′**). Most uPN input was delivered by OSNs (~62% in both glomeruli) and less from MGNs (~36%). The uPN input fraction from other uPNs in DA2 or the autaptic input from the single uPN in DL5 was small (2%; **Figure 5E′′**). The MGNs in DA2 received a smaller fraction of uPN feedback input than in DL5 (17% vs. 26%; **Figure 5E′′**) but a greater OSN input fraction (45% vs. 38%; **Figure 5E′′**). The MGN input from other MGNs was similar in both glomeruli.

To further explore whether differences in circuitry between DA2 and DL5 might represent characteristic features of broad vs. narrowly tuned glomeruli, we analyzed connectome data from another narrowly tuned glomerulus (VA1v; (Horne et al., 2018). We calculated the relative synaptic strength between OSNs (n=107), uPNs (n=5) and MGNs (n=74) in the VA1v (**Figure 5D; Table S2**) (**Figure 5E**). We found that the two narrowly tuned glomeruli shared five circuit features that were different from the broadly tuned glomerulus DL5: (**1**), OSNs in VA1v, as reported above for DA2,

483 displayed a stronger relative feedforward output to uPNs (22%) and to MGNs (32%)
484 (**Figure 5D**). The uPNs and MGNs in VA1v, received a larger fraction of OSN input
485 than in DL5 (**Figure 5E''**). (**2**), the OSN>OSN synaptic output was four times stronger
486 (6%) than in DL5 (1.5%; **Figure 5B-D, Table S1**). This was also reflected in the OSN
487 output fraction to sister OSNs (10%), which in VA1v was more than twice that of DL5
488 (4%; **Figure 5E'**) and in the much greater OSN input fraction (38%) to OSNs in the
489 VA1v than in DL5 (20%; **Figure 5E''**). (**3**), in the VA1v the uPN>uPN relative synaptic
490 output was more than twice that of DL5 (1% vs. 0.4% in DL5; **Figure 5D**), which is in
491 accordance with a much greater uPN output fraction to uPNs (14%) in VA1v than in
492 DL5 (3%) (**Figure 5E'**). (**4**), as observed before in DA2, VA1v uPNs had fewer feedback
493 synapses onto MGNs than in DL5 (relative synaptic strength of uPN>MGN
494 connection: 6% vs. 17%; **Figure 5C-D**), also reflected in a smaller output fraction from
495 uPNs to MGNs in VA1v than in DL5 (81% vs. 96%; **Figure 5E'**). In agreement, the
496 MGN input fraction from uPNs in VA1v was much smaller than in DL5 (10% vs. 26%;
497 **Figure 5E''**). (**5**), OSNs in VA1v received a smaller MGN input fraction than DL5 OSNs
498 (60% vs. 78%; **Figure 5E''**).
499 Besides relative differences (stronger or weaker) in DA2 and VA1v connection
500 motifs compared to DL5, two connection motifs were stronger in DA2 and DL5 but
501 weaker in VA1v: **(1)** the MGN>uPN connection, showing a synaptic strength of 12%
502 and 10% in DA2 and DL5 vs. 8% in VA1v (**Figure 5B-D, Table S2**). In agreement with
503 this, the MGN output fraction to uPNs (**Figure 5E'**, MGN output) and the MGN input
504 fraction in uPNs was greater in DA2 and DL5 than in VA1v (**Figure 5E''**, uPN input).
505 **(2)**, the relative synaptic strength in MGN>MGN motifs was similar between DA2 and
506 DL5 (23%; **Figure 5B-C**), but weaker in VA1v (17%; **Figure 5D, Table S2).** This was
507 also reflected in a smaller MGN output and input fraction from or to MGNs (**Figure**
508 **5E' and E''**).
509 In summary, the two narrowly tuned glomerular circuits studied here shared
510 several circuit features when compared with the broadly tuned glomerular circuit (all
511 glomerular circuit features in DA2, DL5 and VA1v are shown in **Figure 6A**). These
512 features were (1) a stronger OSN>uPN and OSN>MGN connection, (2) a much
513 stronger axo-axonic communication between sister OSNs, (3) a stronger dendro-
514 dendritic connection between uPN dendrites, (4) less feedback from uPNs to MGNs
515 and (5) less feedback from MGNs to OSNs (**Figure 6B**).
516
517 **Autapses in the large DL5 uPN connect distant regions of its dendritic tree**

518 Autapses (synapses made by a neuron upon itself) have seldomly been
519 reported in the *Drosophila* central nervous system (Takemura et al., 2015;Horne et al.,
520 2018). In the DA2 glomerulus we found few autapses in uPNs and MGNs but more in
521 the single DL5 uPN (**Figure 5C; Figure 7A**). In the dendritic tree of the single DL5
522 uPN, on the other hand, three observers registered 54 autaptic connections
523 independently (see Methods). This represents 3% of the output connections of this
524 neuron and 0.4% of all synaptic contacts in the whole glomerulus (**Figure 7A**; **Figure**

525 **5C; E'**). We hypothesized that these autapses could be important for connecting
526 distant parts of this very large dendritic tree. We thus analyzed the exact location and
527 distribution of autaptic presynaptic and postsynaptic sites in this neuron (**Figure 7A**)
528 and found that the autapses along the dendrites of the DL5 uPN were not distributed
529 evenly. Some dendritic branches received several autaptic inputs, whereas other had
530 no autaptic input (**Figure 7A**). We also discovered a difference in the distribution of
531 the pre- and postsynaptic elements of DL5 autapses. Whilst their presynaptic T-bars
532 were evenly distributed at basal (strahler order: 5) and distal regions (strahler order:
533 1-4), 95% of their postsynaptic sites were located at the most distal region (strahler
534 order 2-1; **Figure 7B-C**). We also calculated the geodesic distance (i.e., along-the-arbor
535 distance) from pre- and post-synaptic sites to the basal root node, which is the node
536 point where the uPN enters the glomerulus and is equivalent to the closest point to
537 the soma in our reconstruction. The geodesic distance from the presynaptic site to the
538 basal root node was significantly shorter than the geodesic distance from postsynaptic
539 sites to the basal root node (**Figure 7 – figure supplement 1B**). The pre- and
540 postsynaptic sites of each autapse were either close to each other along the dendritic
541 tree, or distant from each other (see examples in the dendrogram depicted in **Figure**
542 **7D**). Thus, the geodesic distance between pre- and postsynaptic sites, (see scheme in
543 **Figure 7E**), as well as the number of branching points between pre- and postsynaptic
544 partners, were bimodally distributed (**Figure 7F-G**). Autapses that connected distant
545 dendritic subunits were more frequent than those that connected close subunits of the
546 dendrite (**Figure 7E-G**). In summary, we found abundant autapses within the uPN
547 dendrite of DL5. These autapses were unevenly distributed, with many output sites
548 located in a few sub-branches connecting distal dendritic regions.
549

550 **DISCUSSION**

551 We hypothesized that specialized, narrowly tuned glomerular circuits differ in
552 their ultrastructure and microcircuitry from broadly tuned glomerular circuits. By
553 comparing the connectomes of two narrowly tuned olfactory glomeruli with that of a
554 broadly tuned glomerulus, in *Drosophila melanogaster*, we found prominent features of
555 narrowly tuned glomeruli involving synaptic composition, lateralization of sensory
556 input and synaptic circuitry.
557

558 ## Glomerular circuit analysis: a correlative approach

559 The small size of olfactory glomeruli in *Drosophila* gave us the opportunity to
560 reconstruct and analyze the dense connectome of entire glomeruli with volume-based
561 electron microscopy in a reasonable time period. Here we developed a correlative
562 workflow that combines transgenic neuron labeling with near-infra-red-laser-
563 branding for precise volume targeting. We then used FIB-SEM (Bishop et al., 2011) to
564 resolve glomerular networks at the synaptic level. A similar procedure was used
565 recently to investigate single cellular organelles (Ronchi et al., 2021). An advantage of
566 this approach is that it facilitates localization of the volume of interest with high
567 precision and consequently limits the image volume to a minimum and reduces
568 scanning time. At the same time, the limitation in volume is a drawback of our
569 workflow, as it was impossible to reconstruct neurons back to their soma. This fact
570 prevented the identification of individual neurons as in other connectome studies
571 (Berck et al., 2016;Eichler et al., 2017;Horne et al., 2018;Zheng et al., 2018;Bates et al.,
572 2020;Scheffer et al., 2020;Xu et al., 2020;Schlegel et al., 2021).
573 We provide data on innervation and synapse density of olfactory sensory
574 neurons (OSNs), uniglomerular projection neurons (uPNs) and multiglomerular
575 neurons (MGNs) in the *Drosophila* antennal lobe (AL). We observed a higher
576 innervation density of all neuron types but mainly by uPNs and MGNs and in parallel
577 higher density of synaptic contacts along OSN terminals in the narrowly tuned DA2
578 compared with DL5. These results suggest that narrowly tuned glomeruli have a more
579 densely packed neuropil, forming more numerous synaptic connections in the
580 feedforward motifs OSN>uPN and OSN>MGN. Overall, our observations on synapse
581 density were comparable with previous reports (Mosca and Luo, 2014;Rybak et al.,
582 2016;Horne et al., 2018).
583

584 ## Specific features of narrowly tuned glomerular circuits

585 Our analysis revealed circuit features in the narrowly tuned glomerulus DA2
586 and VA1v that might be adaptations specific of such dedicated glomerular circuits.
587 Nevertheless, future studies, analyzing precise numbers of synaptic connections in
588 more individuals, combined with physiological studies and computational models
589 are required to test this hypothesis.

590 **The OSN>uPN feedforward connection is stronger in DA2 and VA1v**

591 OSN presynaptic terminals provide the major input to uPNs in insect olfactory
592 glomeruli (Hansson and Anton, 2000;Chen and Shepherd, 2005;Kazama and Wilson,
593 2008;Lei et al., 2010;Tobin et al., 2017;Horne et al., 2018;Rybak and Hansson,
594 2018;Schlegel et al., 2021). Here we showed that this connection is stronger in DA2 and
595 VA1v than in DL5 (**Figure 5 and 6**). A strong OSNs>uPN synaptic connection will
596 drive non-linear signal amplification, which improves signal detection at low odor
597 concentrations (Ng et al., 2002;Bhandawat et al., 2007;Kazama and Wilson, 2008;Masse
598 et al., 2009). Increasing the number of synapses of this type could have the potential
599 to improve this amplification effect, as shown by artificial increase of synaptic sites in
600 the AL (Acebes and Ferrus, 2001) and in lateral horn dendrites (Liu et al., 2022).
601 Each of the 7 uPNs in DA2 received convergent synaptic input from almost all
602 DA2-OSNs. This is in agreement with reports on the narrowly tuned glomeruli DA1
603 and VA1v (Agarwal and Isacoff, 2011;Jeanne and Wilson, 2015;Horne et al., 2018) and
604 for broadly tuned glomeruli (Vosshall et al., 2000;Chen and Shepherd, 2005;Kazama
605 and Wilson, 2009;Masse et al., 2009;Tobin et al., 2017). High OSN>uPN convergence is
606 the main driver of highly correlated activity among uPNs in pheromone coding
607 glomeruli in flies as well as moths (Kazama and Wilson, 2009;Rospars et al., 2014).
608 High convergence in the lateral horn improves signal transmission from uPNs to
609 lateral horn neurons without sacrificing speed (Jeanne and Wilson, 2015;Huoviala et
610 al., 2020). In the mushroom body calyces, however, the high degree of convergence is
611 only pursued for DA2 uPNs, which converge onto few Kenyon cells, whereas VA1v
612 uPNs randomly synapse onto many dispersed Kenyon cells (Caron 2013; Zheng 2020;
613 Li 2020), indicating diverse signal integration in the mushroom body.
614 From our study, we hypothesize that narrowly tuned glomerular circuits have
615 more uPNs, which have strong convergence onto downstream partners, to improve
616 signal transmission accuracy within a single glomerular circuit. Secondly, a stronger
617 OSN-uPN connection might compensate for the lack of OSN signal transmission sites
618 distributed across glomeruli that are activated by odorants activating multiple
619 broadly tuned OSNs.

620 **Reciprocal connections between sister OSNs and sister uPNs are stronger in**
621 **narrowly tuned glomeruli**

622 The reciprocal OSN-OSN synapse is generally stronger in narrowly tuned
623 glomeruli DA1, DL3 and DL4, compared to broadly tuned glomeruli DL5, DM6, DM3
624 and DM4 (Suh et al., 2004;Knaden et al., 2012;Dweck et al., 2015;Ebrahim et al.,
625 2015;Grabe et al., 2016;Seki et al., 2017;Tobin et al., 2017;Schlegel et al., 2021). A high
626 degree of axo-axonic synapses between sister OSNs was also found in VA1v (Horne
627 et al., 2018;Schlegel et al., 2021)and DA2 but not in the DL5 (this study). Hence, we
628 suggest that a strong OSN-OSN connection is a characteristic feature of the synaptic
629 circuitry of narrowly tuned olfactory glomeruli. Axo-axonic connections have also

630 been reported between gustatory and mechanosensory neurons in *Drosophila* larvae
631 (Miroschnikow et al., 2018) and in the olfactory epithelium and the olfactory bulb of
632 vertebrates (Hirata, 1964;Shepherd et al., 2021). In vertebrates axo-axonic synapses
633 between excitatory sensory neurons are involved in correlated transmitter release
634 (Cover and Mathur, 2021), reminiscent of correlated uPN activity due to reciprocal
635 synaptic and electric coupling in the *Drosophila* AL and LH (Kazama and Wilson,
636 2009;Huoviala et al., 2020). A strong OSN-OSN connection also has the potential to
637 increase the correlation of OSN spiking events and therefore facilitate a robust OSN
638 signal (de la Rocha et al., 2007).
639 Reciprocal dendro-dendritic synapses between sister uPNs of the DA2 have
640 been reported previously also for glomeruli DM6, DM4, VA7 and VA1v (Kazama and
641 Wilson, 2009;Rybak et al., 2016;Tobin et al., 2017;Horne et al., 2018). These types of
642 synapses enhance uPN signal correlation (Kazama and Wilson, 2009), as reported for
643 mitral and tufted cells of the vertebrate olfactory bulb, the circuit equivalent to PNs of
644 insect ALs (Christie et al., 2005;McTavish et al., 2012;Shepherd et al., 2021). In
645 *Drosophila* multiple uPNs could induce correlated PN depolarization events, which
646 improve the signal-to-noise-ratio of PN signal transmission (Chen and Shepherd,
647 2005;Kazama and Wilson, 2009;Jeanne and Wilson, 2015).
648 In summary, our data give evidence that reciprocal OSN-OSN and uPN-uPN
649 connections are a prominent feature of the synaptic circuit of narrowly tuned
650 glomeruli. With stronger OSN>uPN output, we think that reciprocal dendro-dendritic
651 synapses boost signal amplification and neuronal correlation and that this will in turn
652 enhance the signal-to-noise ratio (accuracy) and transmission probability of weak
653 and/or irregular odorant input, increasing processing speed.

654 **Less lateralization in the OSN bilateral connectivity in narrowly tuned glomeruli**

655 In *Drosophila*, most OSN axons project bilaterally and form synapses in their
656 corresponding glomerulus on both the left and right brain hemispheres (Stocker et al.,
657 1990;Vosshall et al., 2000;Couto et al., 2005;Kazama and Wilson, 2009;Silbering et al.,
658 2011;Tobin et al., 2017;Schlegel et al., 2021). This is rarely observed in other insects and
659 absent in vertebrates (Stocker et al., 1983;Masson and Mustaparta, 1990;Galizia et al.,
660 1998;Hansson and Anton, 2000;Anton et al., 2003;Parthasarathy and Bhalla, 2013;Dalal
661 et al., 2020). In the mammalian olfactory system, bilateral comparison of olfactory
662 input only occurs in higher brain centers (Dalal et al., 2020). In flies, bilateral sensory
663 input enables them to discriminate odor sources of different spatial origin through
664 bilateral comparison of olfactory stimulation (Borst and Heisenberg,
665 1982;Duistermars et al., 2009;Gaudry et al., 2013;Mohamed et al., 2019a;Taisz et al.,
666 2022). Asymmetric OSN connectivity, shown for many olfactory OSNs (Tobin et al.,
667 2017;Schlegel et al., 2021) seems to be the origin of a bilateral contrast in the uPN
668 response (Agarwal and Isacoff, 2011;Gaudry et al., 2013;Tobin et al., 2017;Taisz et al.,
669 2022), and is most likely the key to precise odor source localization (Taisz et al., 2022).
670 Bilateral comparison is also used in the lateral horn (a higher olfactory brain center in

671 *Drosophila*) for odorant position coding (Mohamed et al., 2019a). However, not all
672 glomeruli are similar in the magnitude of bilateral asymmetry with respect to their
673 OSN connectivity (Schlegel et al., 2021) or their uPN responses (Agarwal and Isacoff,
674 2011).
675 We found, in agreement with observations in other olfactory glomeruli (Tobin
676 et al., 2017;Schlegel et al., 2021), that glomeruli DL5, DA2 and VA1v (data from:
677 (Horne et al., 2018) have ipsilaterally asymmetric OSN synaptic output to excitatory
678 uPNs and sister OSNs and contralaterally an enhanced OSN>MGN output (**Figure 4**).
679 We believe that, in agreement with a recent study, these asymmetric connections
680 determine a strong left-right-contrast in the uPN response, akin to a "winner-takes-
681 all" principle (Taisz et al., 2022).
682 We also observed that the degree of bilateral OSN asymmetry in DA2 and
683 VA1v was much weaker than in DL5 (**Figure 4**). Weakly lateralized OSN connectivity
684 is perhaps insufficient to induce an adequate bilateral contrast necessary for odor
685 source localization. Recent work supports this idea by showing the importance of the
686 interplay of asymmetric OSN signaling and LN inhibition to enhance the bilateral
687 contrast of uPN activity and to facilitate navigation (Taisz et al., 2022).
688 Why do these narrowly tuned glomeruli have weaker bilateral contrast than
689 broadly tuned glomeruli? The answer could lie in the ecological significance of the
690 individual odorants. Geosmin, encoded by glomerulus DA2 (Stensmyr et al., 2012),
691 and the pheromone methyl laurate, encoded by glomerulus VA1v (Dweck et al.,
692 2015), act at short distances, mainly when the fly is walking and not flying, influencing
693 either oviposition or aggregation behavior in females. Perhaps, the decision between
694 avoiding and staying when geosmin or methyl laurate are detected does not need a
695 precise odor source location, as is the case for food odorants. Food odor detection,
696 which happens mainly at flying conditions, needs continuous processing of odor
697 position and body alignment to navigate towards the odor source (Thoma et al.,
698 2015;Demir et al., 2020). The bilateral OSN projection onto uPNs in DA2 and VA1v
699 potentially has a distinct function other than odor position coding and could, via the
700 enhancement of the effect of convergence of OSN>uPN signal transmission, enhance
701 odor signal amplification (Bhandawat et al., 2007;Kazama and Wilson, 2009;Masse et
702 al., 2009;Jeanne and Wilson, 2015)

703 **Distinct synaptic integration of local modulatory neurons in narrowly tuned**
704 **glomeruli**

705 MGNs are composed of multiglomerular projection neurons (mPNs) that
706 project directly to the LH (Jefferis et al., 2007;Strutz et al., 2014;Bates et al., 2020) and
707 inhibitory and excitatory local interneurons (LNs) that interconnect the AL glomeruli
708 (Masse et al., 2009;Okada et al., 2009;Chou et al., 2010;Seki et al., 2010;Liu and Wilson,
709 2013). Since LNs are the most numerous and broadly arborizing of the
710 multiglomerular cell types in the AL (Chou et al., 2010;Lin et al., 2012), we focus our
711 discussion on these. Multiglomerular LNs are crucial in modulation of the OSN>uPN

signal transmission (Masse et al., 2009;Chou et al., 2010;Seki et al., 2010;Galizia, 2014;Szyszka and Galizia, 2015).

Previous observations have shown that glomeruli DA2 and VA1v have a lower number of innervating LNs (Chou et al., 2010;Grabe et al., 2016) and receive less global interglomerular LN inhibition than broadly tuned glomeruli (Hong and Wilson, 2015). We therefore assumed that DA2 or VA1v would have a lower LN innervation density and less LN synaptic integration in their circuitry. However, we did not observe a general lower synaptic integration in DA2 (**Figure 5**) and found a greater MGN innervation density, and a higher density of input sites than in DL5. VA1v MGNs on the other hand received less synaptic input and provided less output in its glomerular circuit than MGNs in DL5.

Taking a closer look at particular synaptic connection motifs of MGNs we saw that narrowly tuned glomeruli had a weak uPN>MGN feedback (**Figure 6**). uPN feedback onto LNs and their reciprocal connection (LN>uPN) was reported in *Drosophila* and other insects, such as honey bees, cockroaches and moths, but its function is still poorly understood (Boeckh and Tolbert, 1993;Sun et al., 1997;Sachse and Galizia, 2002). In *Apis mellifera* reciprocal dendro-dendritic synapses between excitatory and inhibitory neurons enhance signal contrast and the reliability of true signal representations throughout the AL (Yokoi et al., 1995;Sachse and Galizia, 2002). Here we could not differentiate the LN types involved in the uPN>MGN synaptic motif. However, the prevailing uPN>LN synapses involve mainly widespread pan-glomerular LNs in the adult (Horne et al., 2018) and larval AL (Berck et al., 2016), which are important for combinatorial coding (Galizia, 2014;Sachse and Hansson, 2016). Thus, weaker uPN>MGN feedback in the narrowly tuned DA2 and VA1v circuits might be a compensatory mechanism to lower the computational demand of interglomerular communication for odor identity coding.

We also observed that OSNs in the narrowly tuned DA2 and VA1v received less MGN input than the OSNs of the DL5, suggesting that the OSNs in DA2 and VA1v receive relatively weak presynaptic inhibition. Pan-glomerular GABAergic LNs induce presynaptic inhibition at OSN presynaptic site (Berck et al., 2016;Schlegel et al., 2021). These inhibitory LNs are drivers of balanced glomerular gain control and are a key player for odor identity coding, balancing incoming and alternating odor intensities (Olsen and Wilson, 2008;Root et al., 2008;Silbering et al., 2008;Asahina et al., 2009;Wang, 2012;Galizia, 2014;Hong and Wilson, 2015;Szyszka and Galizia, 2015;Sachse and Hansson, 2016). Our data support these observations and provide an argument for why narrowly tuned OSNs receive much lower inhibition during AL stimulation with odorants activating other OSN populations (Hong and Wilson, 2015). Even though DA2 and VA1v might receive less interglomerular inhibition, their OSN>MGN output is still strong, in agreement with studies showing that throughout the AL, global lateral inhibition, mediated by LNs, scales with general OSN activation (Olsen and Wilson, 2008;Hong and Wilson, 2015).

In summary, narrowly tuned circuits are probably influenced more strongly by intraglomerular than by interglomerular modulation. Narrowly tuned circuits

755 perhaps have greater computational capacities in intraglomerular modulation of
756 signal transmission, which could be important for example for PN fine-tuning and
757 response adjustment (Ng et al., 2002;Assisi et al., 2012).
758 Above we discussed putative generic features of narrowly tuned glomerular
759 circuits. Besides these circuit features, we found a strong MGN>MGN connection in
760 the aversive glomerular circuits DA2 and DL5 in contrast to a much weaker
761 MGN>MGN connection in the attractive glomerulus VA1v (Knaden et al.,
762 2012;Stensmyr et al., 2012;Knaden and Hansson, 2014;Dweck et al., 2015;Mohamed et
763 al., 2019b). Why do aversive olfactory circuits have a stronger MGN-MGN connection
764 than attractive circuits? In the larval *Drosophila* AL, reciprocal LN-LN synapses induce
765 disinhibition induced by a strong connection between the pan-glomerular LNs and a
766 bilateral projecting LN, the Keystone LN, which synapses strongly onto pan-
767 glomerular LNs and selectively onto OSNs, which are activated by attractive food
768 odors. This is thought to be a key feature to switch from homogenous to
769 heterogeneous presynaptic inhibition and therefore to a selective gain control
770 enhancing contrast between attractive and aversive odor activation (Berck et al., 2016).
771 Such balanced inhibitory systems could also be present in the adult *Drosophila* AL,
772 reflected in the strong LN-LN connection in DA2 and DL5. Disinhibition of
773 interglomerular presynaptic inhibition in aversive glomeruli circuits might be
774 important for the fly to stay vigilant to aversive odors, while perceiving attractive
775 cues, for example during feeding conditions so that a fast switch in behavior can be
776 initiated.
777

778 **Autaptic connection within the dendritic tree of a single uPN**

779 We observed autapses along the large dendritic tree of the single DL5-uPN. To
780 our knowledge, this is the first report of bulk dendro-dendritic autapses in the
781 *Drosophila* olfactory system, indicating a cell-type specific occurrence of autapses in
782 the DL5-uPN as reported for certain cell types of the optic lobe (Takemura et al., 2015).
783 Autapses are also reported to be present at different frequencies in different types of
784 neurons in the mammalian brain (Van der Loos and Glaser, 1972;Tamás et al.,
785 1997;Bekkers, 1998;Bacci and Huguenard, 2006;Ikeda and Bekkers, 2006;Bekkers,
786 2009;Saada et al., 2009). In *Drosophila,* most uPNs are cholinergic (Yasuyama and
787 Salvaterra, 1999;Yasuyama et al., 2003;Kazama and Wilson, 2008;Tanaka et al.,
788 2012;Croset et al., 2018) and DL5-uPN autapses might activate either nicotinic or
789 muscarinic acetylcholine postsynaptic receptors**.** Muscarinic acetylcholine receptors
790 have an inhibitory effect in the Kenyon cells of the mushroom body (Bielopolski et al.,
791 2019), but mediate excitation in the AL (Rozenfeld et al., 2019)**.**
792 What is the function of these autaptic feedback loops within a DL5-uPN
793 dendrite? Recent studies in vertebrates show that excitatory autapses enhance neuron
794 bursting and excitability (Guo et al., 2016;Wiles et al., 2017;Yin et al., 2018). Autaptic
795 inhibitory connections have been implicated in circuit synchronization, spike-timing
796 precision, self-stabilization of neuronal circuits and feedback inhibition (Ikeda and

797 Bekkers;Van der Loos and Glaser, 1972;Tamás et al., 1997;Bekkers, 1998;Bacci and
798 Huguenard, 2006;Saada et al., 2009).
799 Autapses in the DL5 uPN form mainly long-distance feedback loops,
800 connecting distinct dendritic subtrees and the basal dendrite region (closer to the
801 soma) with distal branches. This spatial segregation is similar to the distribution of
802 non-autaptic pre- and postsynaptic sites in *Drosophila* uPNs, where presynapses are
803 located more frequently at basal dendrites than postsynapses (Rybak et al., 2016) and
804 other insects, such as *Periplaneta americana* and moths (Malun, 1991;Sun et al., 1997;Lei
805 et al., 2010). Dendro-dendritic autaptic feedback loops connecting basal to distal
806 branches and distinct dendritic subtrees of a large dendritic tree might facilitate
807 activity correlation between distant dendritic subunits, as described for non-autaptic,
808 reciprocal uPN-uPN connections (Kazama and Wilson, 2009). This could be important
809 in a large compartmentalized dendrite that receives inhomogeneous excitation by
810 several OSNs at distinct dendritic sites, in order to enhance synchronized
811 depolarization events along the dendrite, supporting signal integration (Graubard et
812 al., 1980;Tran-Van-Minh et al., 2015). Clustered autapses could mediate local signal
813 input amplification for distinct dendritic subunits (Kumar et al., 2018;Liu et al., 2022).
814 Autaptic contacts, finally, could be able to shift the uPN membrane depolarization
815 towards the spiking threshold, and enhance the firing probability during activation.
816 In conclusion, we provide a comprehensive comparative analysis of the
817 ultrastructure and synaptic circuitry of two functionally diverse olfactory glomeruli
818 with distinct computational demands, processing either single odorant information in
819 a dedicated olfactory pathway (DA2) or input regarding several odorants and taking
820 part in combinatory coding across distributed glomeruli (DL5). Our work provides an
821 opportunity to gain insight into variations in network architecture and provides
822 fundamental knowledge for future understanding of glomerular processing. By
823 comparing our data with those from another narrowly tuned glomerulus (VA1v), we
824 distilled prominent circuit features that suggest that narrowly tuned glomerular
825 circuits encode odor signals with a weaker left-right-contrast, improved accuracy,
826 stronger signal amplification and stronger intraglomerular signal modulation relative
827 to broadly tuned glomeruli. Our findings reveal the existence of autapses in olfactory
828 glomeruli and indicate that dendro-dendritic autapses play an important role in
829 dendritic signal integration.
830

831 **Acknowledgments**

832 The authors are most grateful to Michael Steinert and Thomas Pertsch for their
833 support and advice of the FIB-SEM imaging, Katrin Buder for the support with
834 electron microscopy, and Veit Grabe for advice on two-photon imaging. Great
835 thanks also to Albert Cardona for discussion on synaptic networks, him, and Tom
836 Kazimiers (Kazmos GmbH) for the instruction of CATMAID. The neuronal
837 reconstructions were conducted with the outstanding support of Damilola E.
838 Akinyemi, Eckard E. Schumann, and Michael Adewoye. We thank Martin Nawrot

and Magdalena Springer for constructive comments and discussions about autapses. The work was supported by Roland Kilper and Ute Müller, (aura optics, Jena), the European Regional Development Fund, by funds from the DFG (grant no. 430592330), in the Priority Program 'Evolutionary Optimisation of Neuronal Processing' (DFG-SPP 2205) and by the Max Planck Society.

844 **MATERIAL AND METHODS**

845 **Fly line and fly rearing**
846 Flies of the genotype *Orco-GAL4; UAS-GCaMP6s* were obtained from the Bloomington
847 *Drosophila* Stock Center (https://bdsc.indiana.edu) and reared on standard *Drosophila*
848 food at 25°C and 70% humidity on a 12 h:12 h day:night cycle. Seven-days old female
849 flies were used. In these flies, Orco-positive olfactory sensory cells emit green
850 fluorescence, making possible to identify individual glomeruli.
851
852 **Brain dissection and fixation for Focus Ion Beam microscopy**
853 Two 7-day old female flies were anesthetized with nitric oxide (with Sleeper TAS;
854 INJECT+MATIC, Switzerland) and decapitated with forceps. Heads were dipped for
855 one minute in 0.05% Triton X-100 in 0.1M Sorensen's phosphate buffer, pH 7.3 and
856 transferred to a droplet of freshly prepared ice-cooled fixative (2.5% glutaraldehyde
857 and 2.0% paraformaldehyde in 0.1M Sørensen's phosphate buffer, pH 7.3; as in
858 (Karnovsky, 1965). The proboscis was removed and the back of the head was opened
859 to improve fixative penetration. After 5-10 minutes, the brain was dissected out of the
860 head capsule and post-fixed for two hours on ice. Fixation was stopped by rinsing the
861 brain several times in ice-cooled 0.1M Sørensen's phosphate buffer, pH 7.3 (after
862 (Rybak et al., 2016)).
863
864 **Laser branding of glomeruli for identification during FIB microscopy**
865 To identify the glomeruli of interest at the ultrastructural level and to limit to a
866 minimum the volume of tissue to be scanned with FIB, near-infrared laser branding
867 (NIRB, (Bishop et al., 2011)). Glomeruli of interest were first located with light
868 microscopy in brains of *Orco-GAL4; UAS-GCaMP6s* flies using a confocal microscope
869 (ZEISS LSM 710 NLO, Carl Zeiss, Germany), a 40x water immersion objective (W Plan-
870 Apochromat 40x/1.0 DIC VIS-IR, Carl Zeiss, Jena, Germany), a laser wavelength of 925
871 nm at 30% laser power and ZEN software (Carl Zeiss, Germany). Once glomeruli DA2
872 or DL5 were identified by means of location, shape and size the volume of interest
873 (VOI) was tagged with fiducial marks ("laser-branded") close to the borders of the
874 glomerulus (**Figure 1A-B**), using an infrared Chameleon Ultra diode-pumped laser
875 (Coherent, Santa Clara, USA) at wavelength 800 nm and at 75-90% of laser
876 power).Two laser scan rounds were performed for each induced fiducial brand. DA2
877 (right AL) and DL5 (left AL) were laser-branded in the same fly. A second glomerulus
878 DA2 was marked in the right AL of another fly.
879
880 **Transmission Electron Microscopy**
881 Brains were rinsed with 2.5% sodium-cacodylate buffer and incubated in 1% uranyl
882 acetate in 50% acetone for 30 minutes in the dark for *en bloc* staining. They were then
883 dehydrated with a graded ascending acetone series (30%-100%) and gradually
884 infiltrated with Araldites (glycerol-based aromatic epoxy resins; Serva, Germany). In
885 the final step, the tissue was embedded in pure resin and left in a 60°C incubator to

886 polymerize for 48h. Resin blocks were trimmed with a Reichert UltraTrim microtome
887 (Leica, USA) and the fiducial laser marks were then located in semi-thin sections. To
888 check tissue quality before performing high-resolution volume based electron
889 microscopy, serial sections 50 nm in thickness were cut with a diamond knife (Ultra
890 45°, Diatome, Switzerland) on a Reichert Ultracut S ultramicrotome (Leica, Germany),
891 collected on single slot grids (2 x 1 mm), and imaged with a JEM 1400 electron
892 microscope (Jeol, Germany) operated at 80 kV. Digital micrographs were obtained
893 with a Gatan Orius SC 1000 CCD camera (Gatan Orius SC 1000; Gatan, USA)
894 controlled with the Gatan Microscopy Suite software Vers. 2.31.734.0.
895 .

896 **Focused Ion Beam-Scanning Electron Microscopy (FIB-SEM)**

897 Before serial Focused Ion Beam Scanning Electron Microscopy imaging (FIB-SEM;
898 (Knott et al., 2008;Xu et al., 2017), the surface of the trimmed block was coated with a
899 conductive layer of carbon to prevent charging artifacts. The VOIs were imaged using
900 a FEI Helios NanoLab G3 UC equipment (FEI, USA). The laser marks used to
901 landmark the VOI were visible across the surface of the block. The VOI surface was
902 protected via a local electron beam and subsequently, an ion beam deposition of
903 platinum was applied using a gas injection system to remove surrounding material
904 and to reduce re-deposition. Serial images across the entire VOI were generated by
905 repeated cycles of milling and imaging, orthogonal to the block surface. The tissue
906 was milled with a focused beam of gallium ions using FEI's Tomahawk ion column
907 (accelerating voltage: 30 kV, beam current: 790 pA, milling steps: 20 nm). After each
908 milling cycle, the back-scattering electrons were detected with an in-column detector
909 (FEI's Elstar electron column operating at 3kV accelerating voltage; 1.6 nA beam
910 current; 10 µs dwell time) used to create an image of the newly exposed surface during
911 each scan cycle. The DA2 and DL5 volumes (DA2: 769 slices; DL5: 976 slices) in the
912 first fly were imaged with a pixel resolution of 4.9 x 4.9 x 20 nm/pix (pixel field: 4096
913 x 3536 (DA2) and 5218 x 3303 (DL5). The dataset of the DA2 volume (571 slices) in a
914 second fly was imaged with a pixel resolution of 4.4 x 4.4 x 20 nm/pix (pixel field: 4096
915 x 3536). The milling/imaging cycles were controlled with the FEI Auto Slice and View
916 operating 4.0 software (FEI).
917

918 **Image alignment, 3D reconstruction and segmentation**

919 FIB-SEM image stacks were aligned by maximizing the Pearson correlation coefficient
920 of the central part of two consecutive images using template matching from the
921 openCV library (https://opencv.org). Dense reconstruction of the glomeruli were
922 produced by manually tracing all neuronal fibers and by annotating all synapses
923 within the two glomeruli, using a skeleton-based reconstruction procedure similar to
924 previous approaches (Berck et al., 2016;Schneider-Mizell et al., 2016;Zheng et al.,
925 2017). Up to five independent tracers and two reviewers participated in an iterative
926 reconstruction process using the web-based reconstruction software CATMAID
927 (http://www.catmaid.org; RRID:SCR_006278; (Saalfeld et al., 2009;Schneider-Mizell et
928 al., 2016); **Figure 1D, Figure 1 -- video 1**), performing a dense reconstruction of a

929 synaptic neuropil. In a another fly, neurons of a DA2 glomerulus were manually
930 reconstructed with the volume-based reconstruction method TrakEM2 (Cardona et
931 al., 2012), an ImageJ (Fiji) plugin (https://imagej.net/TrakEM2).
932
933 **Glomerular border definition**
934 The definition of the boundary between olfactory glomeruli was based on the
935 combination of several structural features: the spatial position of pre- and
936 postsynaptic elements along OSN axons, the position of the majority of uPN
937 postsynaptic sites, the faint glial leaflets scattered at the periphery of the glomerulus,
938 and the fiducial laser marks (**Figure 1B, D**).
939
940 **Neuron identification**
941 Neuronal fibers were assigned to one of three pre-defined neuron classes: OSNs,
942 uPNs, and MGNs. The classification was based on their 3D shape (**Figure 2A**), their
943 branching intensity (**Figure 2B**), the average diameter of their fibers (neuronal profiles:
944 **Figure 2A -** FIB-SEM image; exemplary volume based reconstruction), the ratio of T-
945 bars-to-input sites and the size of their T-bars, which were either "small" (few
946 postsynaptic connections) or "large" (many postsynaptic connections **Figure 2 –**
947 **supplement 1B-D)**. In addition, several intracellular features helped to classify neuron
948 classes: the shape and appearance of mitochondria, the size and electron density of
949 vesicles and the amount of spinules (small filopodia-like invaginations of neighboring
950 cells (**Figure 2A -** FIB-SEM image; (Gruber et al., 2018). OSNs and uPNs could be
951 counted, due to their uniglomerular character, by means of the identification of the
952 axons (OSNs) or main dendrites (uPNs) entering the glomerulus. The number of
953 MGNs could not be counted because of their pan-glomerular projection patterns in
954 the AL. Ipsi- and contralateral OSNs in DA2 and DL5 were identified based on the
955 trajectory of axonal fibers and their entry location in each glomerulus, (example
956 neurons: **Figure 4B).** Ipsilateral OSNs reach the glomerulus from the ipsilateral
957 antennal nerve and leave the glomerulus towards the antennal lobe commissure
958 (ALC: (Tanaka et al., 2012)). Contralateral OSNs reach the glomerulus projecting from
959 the ALC.
960
961 **Data analysis**
962 With the aid of the web-based software CATMAID (http://www.catmaid.org), we
963 traced neurons in each VOI and the following properties were quantified: the
964 glomerular volume, neuronal fiber length (in µm), number of fiber branching points,
965 number of synaptic input and output sites and T-bars (see data availability). In a
966 second fly, the volume of neurons in DA2 was measured with the aid of TrakEM2
967 (Cardona et al., 2012), an ImageJ (Fiji) plugin (https://imagej.net/TrakEM2). The
968 following calculations were performed:
969 1. $Innervation\ density = \frac{total\ neuron\ length\ (\mu m)}{glomerular\ volume\ (\mu m^3)}$,

970 a. calculated as a ratio: (1)the sum of all neuronal fibers of each neuron
971 class or (2) all together (**Table 1**) or (3) for each neuron individually
972 (**Figure 3**)

973 2. $Glomerular\ synaptic\ density = \frac{\#\ of\ synaptic\ inputs,-\ \ outputs\ or\ T-bars}{glomerular\ volume\ (\mu m^3)}$,

974 a. calculated as a ratio: (1) the sum of all neuronal fibers of each neuron
975 class or (2) all together (**Table 1**) or (3) for each neuron individually
976 (**Figure 3**)

977 3. $Neuronal\ synaptic\ density = \frac{\#\ of\ synaptic\ inputs-,outputs\ or\ T-bars}{neuronal\ fiber\ length\ (\mu m)}$ (**Table 1;**
978 **Figure 3 – figure supplement 1**)

979 4. $Synaptic\ ratios = \frac{\#\ of\ T-bars\ or\ outputs}{inputs}$ (represents the average for each neuron
980 class; **Table 1**)

981 5. $Polyadicity = \frac{\#\ of\ outputs}{T-bars}$ (represents the average number of postsynaptic sites
982 at a T-bar of each neuron class; **Table 1 and Figure 1E**)

983 6. Relative differences $= \frac{respective\ value\ target\ glomerulus-value\ \ source\ \ glomerulus}{source\ glomerulus} \times$
984 100 (**Table S1; Table S2**)

985 7. Relative synaptic strength $= \frac{\#\ of\ synaptic\ contacts\ from\ neuron\ class\ A\ to\ B}{\#\ all\ synaptic\ contacts\ in\ corresponding\ glomerulus}$ (**Table**
986 **S1; Table S2**)

987 8. Fraction of output $= \frac{\#\ of\ outputs\ of\ neuron\ class\ A\ directed\ to\ neuron\ class\ B}{total\ \#\ of outputs\ of\ neuron\ class\ A} \times\ 100$

988 9. Fraction of input $= \frac{\#\ of\ \ inputs\ from\ neuron\ class\ A\ from\ class\ B}{total\ \#\ of\ inputs\ of\ neuron\ class\ A} \times\ 100$

989 Graphs were made with the programming language R and RStudio (R Core Team,
990 2018) using the packages 'ggplot2' and 'reshape' (see data availability) or with Python
991 (see data availability). All figures were compiled with Adobe Illustrator CS5 software
992 (Adobe Inc.).
993 Statistical analysis was performed with R Studio (R Studio Team, 2016) using the
994 packages 'ggsignif'. Differences between samples DA2 and DL5 or between ipsilateral
995 and contralateral OSNs were tested for significance with a two-sided student's t-test
996 if sample size was normally distributed, or with Wilcoxon two sample test if the data
997 was not normally distributed (noted in figure legend). Data is in all cases represented
998 as mean + standard deviation.
999

1000 ## Analysis of autapses

1001 The location of autapses, the measurement of their geodesic (distance along the
1002 neuronal dendrite) and the number of branching points from point A (presynaptic
1003 site) to B (postsynaptic profile) was analyzed with Python using the package
1004 'neuroboom' https://github.com/markuspleijzier/neuroboom (see also data
1005 availability).
1006

1007 ## Data availability

Datasets will be available through the public CATMAID instance: https://catmaid.ice.mpg.de/catmaid_2020.02.15/#. Neurons are named according to their neuron classification. All data and source code packages used in this study are hosted on GitHub: https://github.com/. The neuroboom Python package was used for dendrogram analysis, available at https://github.com/markuspleijzier/neuroboom and https://pypi.org/project/neuroboom/.

1014 **REFERENCES**

1015 Acebes, A., and Ferrus, A. (2001). Increasing the Number of Synapses Modifies
1016 Olfactory Perception in Drosophila. *Journal of Neuroscience* 21, 6264–6273.
1017 Agarwal, G., and Isacoff, E. (2011). Specializations of a pheromonal glomerulus in
1018 the Drosophila olfactory system. *Journal of Neurophysiology* 105, 1711-1721.
1019 Ai, H., and Hagio, H. (2013). Morphological analysis of the primary center receiving
1020 spatial information transferred by the waggle dance of honeybees. *Journal of*
1021 *Comparative Neurology* 521, 2570-2584.
1022 Andersson, M.N., Löfstedt, C., and Newcomb, R.D. (2015). Insect olfaction and the
1023 evolution of receptor tuning. *Frontiers in Ecology and Evolution* 3.
1024 Anton, S., Van Loon, J.J., Meijerink, J., Smid, H.M., Takken, W., and Rospars, J.P.
1025 (2003). Central projections of olfactory receptor neurons from single antennal
1026 and palpal sensilla in mosquitoes. *Arthropod Struct Dev* 32, 319-327.
1027 Asahina, K., Louis, M., Piccinotti, S., and Vosshall, L.B. (2009). A circuit supporting
1028 concentration-invariant odor perception in Drosophila. *J Biol* 8, 9.
1029 Assisi, C., Stopfer, M., and Bazhenov, M. (2012). Excitatory Local Interneurons
1030 Enhance Tuning of Sensory Information. *PLOS Computational Biology* 8,
1031 e1002563.
1032 Auer, T.O., Khallaf, M.A., Silbering, A.F., Zappia, G., Ellis, K., Álvarez-Ocaña, R.,
1033 Arguello, J.R., Hansson, B.S., Jefferis, G.S.X.E., Caron, S.J.C., Knaden, M., and
1034 Benton, R. (2020). Olfactory receptor and circuit evolution promote host
1035 specialization. *Nature*.
1036 Bacci, A., and Huguenard, J.R. (2006). Enhancement of spike-timing precision by
1037 autaptic transmission in neocortical inhibitory interneurons. *Neuron* 49, 119-
1038 130.
1039 Bates, A.S., Schlegel, P., Roberts, R.J.V., Drummond, N., Tamimi, I.F.M., Turnbull, R.,
1040 Zhao, X., Marin, E.C., Popovici, P.D., Dhawan, S., Jamasb, A., Javier, A.,
1041 Serratosa Capdevila, L., Li, F., Rubin, G.M., Waddell, S., Bock, D.D., Costa, M.,
1042 and Jefferis, G. (2020). Complete Connectomic Reconstruction of Olfactory
1043 Projection Neurons in the Fly Brain. *Curr Biol* 30, 3183-3199 e3186.
1044 Bekkers, J.M. (1998). Neurophysiology: are autapses prodigal synapses? *Curr Biol* 8,
1045 R52-55.
1046 Bekkers, J.M. (2009). Synaptic Transmission: Excitatory Autapses Find a Function?
1047 *Current Biology* 19, R296-R298.
1048 Benton, R., Sachse, S., Michnick, S.W., and Vosshall, L.B. (2006). Atypical Membrane
1049 Topology and Heteromeric Function of *Drosophila* Odorant Receptors In Vivo.
1050 *PLoS Biol* 4, 240-257.
1051 Berck, M.E., Khandelwal, A., Claus, L., Hernandez-Nunez, L., Si, G., Tabone, C.J., Li,
1052 F., Truman, J.W., Fetter, R.D., Louis, M., Samuel, A.D.T., and Cardona, A.
1053 (2016). The wiring diagram of a glomerular olfactory system. *eLife* 5, e14859.
1054 Bhandawat, V., Olsen, S.R., Gouwens, N.W., Schlief, M.L., and Wilson, R.I. (2007).
1055 Sensory processing in the *Drosophila* antennal lobe increases reliability and

separability of ensemble odor representations. *Nature neuroscience* 10, 1474-1482.

Bielopolski, N., Amin, H., Apostolopoulou, A.A., Rozenfeld, E., Lerner, H., Huetteroth, W., Lin, A.C., and Parnas, M. (2019). Inhibitory muscarinic acetylcholine receptors enhance aversive olfactory learning in adult Drosophila. *Elife* 8.

Bishop, D., Nikic, I., Brinkoetter, M., Knecht, S., Potz, S., Kerschensteiner, M., and Misgeld, T. (2011). Near-infrared branding efficiently correlates light and electron microscopy. *Nat Meth* 8, 568-570.

Boeckh, J., Distler, P., Ernst, K.D., Hösl, M., and Malun, D. (1990). "Olfactory bulb and antennal lobe," in *NATO ASI Series, Vol. H39: Chemosensory Information Processing,* ed. D. Schild. (Berlin, Heidelberg: Springer Verl), 201-227.

Boeckh, J., and Tolbert, L.P. (1993). Synaptic organization and development of the antennal lobe in insects. *Microscopy research and technique* 24, 260-280.

Borst, A., and Heisenberg, M. (1982). Osmotropotaxis inDrosophila melanogaster. *Journal of comparative physiology* 147, 479-484.

Briggman, K.L., and Denk, W. (2006). Towards neural circuit reconstruction with volume electron microscopy techniques. *Curr Opin Neurobiol* 16, 562-570.

Butcher, N.J., Friedrich, A.B., Lu, Z., Tanimoto, H., and Meinertzhagen, I.A. (2012). Different classes of input and output neurons reveal new features in microglomeruli of the adult *Drosophila* mushroom body calyx. *J Comp Neurol* 520, 2185-2201.

Cardona, A., Saalfeld, S., Schindelin, J., Arganda-Carreras, I., Preibisch, S., Longair, M., Tomancak, P., Hartenstein, V., and Douglas, R.J. (2012). TrakEM2 Software for Neural Circuit Reconstruction. *PLoS One* 7, e38011.

Cardona, A., Saalfeld, S., Tomancak, P., and Hartenstein, V. (2009). *Drosophila* brain development: closing the gap between a macroarchitectural and microarchitectural approach. *Cold Spring Harb Symp Quant Biol* 74, 235-248.

Chen, W.R., and Shepherd, G.M. (2005). The olfactory glomerulus: A cortical module with specific functions. *Journal of Neurocytology* 34, 353–360.

Chou, Y.H., Spletter, M.L., Yaksi, E., Leong, J.C., Wilson, R.I., and Luo, L. (2010). Diversity and wiring variability of olfactory local interneurons in the *Drosophila* antennal lobe. *Nature neuroscience* 13, 439-449.

Christie, J.M., Bark, C., Hormuzdi, S.G., Helbig, I., Monyer, H., and Westbrook, G.L. (2005). Connexin36 mediates spike synchrony in olfactory bulb glomeruli. *Neuron* 46, 761-772.

Coates, K.E., Calle-Schuler, S.A., Helmick, L.M., Knotts, V.L., Martik, B.N., Salman, F., Warner, L.T., Valla, S.V., Bock, D.D., and Dacks, A.M. (2020). The Wiring Logic of an Identified Serotonergic Neuron That Spans Sensory Networks. *The Journal of Neuroscience* 40, 6309-6327.

Couto, A., Alenius, M., and Dickson, B.J. (2005). Molecular, anatomical, and functional organization of the *Drosophila* olfactory system. *Current biology* 15, 1535-1547.

1099 Cover, K.K., and Mathur, B.N. (2021). Axo-axonic synapses: Diversity in neural
1100 circuit function. *J Comp Neurol* 529**,** 2391-2401.
1101 Croset, V., Treiber, C.D., and Waddell, S. (2018). Cellular diversity in the Drosophila
1102 midbrain revealed by single-cell transcriptomics. *Elife* 7.
1103 Cuntz, H., Borst, A., and Segev, I. (2007). Optimization principles of dendritic
1104 structure. *Theor Biol Med Model* 4**,** 21.
1105 Dacks, A.M., Christensen, T.A., and Hildebrand, J.G. (2006). Phylogeny of a
1106 serotonin-immunoreactive neuron in the primary olfactory center of the insect
1107 brain. *J Comp Neurol* 498**,** 727-746.
1108 Dalal, T., Gupta, N., and Haddad, R. (2020). Bilateral and unilateral odor processing
1109 and odor perception. *Commun Biol* 3**,** 150.
1110 Datta, S.R., Vasconcelos, M.L., Ruta, V., Luo, S., Wong, A., Demir, E., Flores, J.,
1111 Balonze, K., Dickson, B.J., and Axel, R. (2008). The *Drosophila* pheromone cVA
1112 activates a sexually dimorphic neural circuit. *Nature* 452**,** 473-477.
1113 De Bruyne, M., Clyne, P.J., and Carlson, J.R. (1999). Odor coding in a model olfactory
1114 organ: the *Drosophila* maxillary palp. *Journal of Neuroscience* 19**,** 4520-4532.
1115 De Bruyne, M., Foster, K., and Carlson, J.R. (2001). Odor Coding in the *Drosophila*
1116 Antenna. *Neuron* 30**,** 537-552.
1117 De La Rocha, J., Doiron, B., Shea-Brown, E., Josić, K., and Reyes, A. (2007).
1118 Correlation between neural spike trains increases with firing rate. *Nature* 448**,**
1119 802-806.
1120 Demir, M., Kadakia, N., Anderson, H.D., Clark, D.A., and Emonet, T. (2020).
1121 Walking Drosophila navigate complex plumes using stochastic decisions
1122 biased by the timing of odor encounters. *Elife* 9.
1123 Dolan, M.-J., Frechter, S., Bates, A.S., Dan, C., Huoviala, P., Roberts, R.J.V., Schlegel,
1124 P., Dhawan, S., Tabano, R., Dionne, H., Christoforou, C., Close, K., Sutcliffe,
1125 B., Giuliani, B., Li, F., Costa, M., Ihrke, G., Meissner, G.W., Bock, D.D., Aso, Y.,
1126 Rubin, G.M., and Jefferis, G.S.X.E. (2019). Neurogenetic dissection of the
1127 Drosophila lateral horn reveals major outputs, diverse behavioural functions,
1128 and interactions with the mushroom body. *eLife* 8**,** e43079.
1129 Dolan, M.J., Belliart-Guérin, G., Bates, A.S., Frechter, S., Lampin-Saint-Amaux, A.,
1130 Aso, Y., Roberts, R.J.V., Schlegel, P., Wong, A., Hammad, A., Bock, D., Rubin,
1131 G.M., Preat, T., Plaçais, P.Y., and Jefferis, G. (2018). Communication from
1132 Learned to Innate Olfactory Processing Centers Is Required for Memory
1133 Retrieval in Drosophila. *Neuron* 100**,** 651-668.e658.
1134 Duistermars, B.J., Chow, D.M., and Frye, M.A. (2009). Flies require bilateral sensory
1135 input to track odor gradients in flight. *Current Biology* 19**,** 1301-1307.
1136 Dweck, H.K.M., Ebrahim, S.a.M., Thoma, M., Mohamed, A.a.M., Keesey, I.W., Trona,
1137 F., Lavista-Llanos, S., Svatoš, A., Sachse, S., Knaden, M., and Hansson, B.S.
1138 (2015). Pheromones mediating copulation and attraction in *Drosophila*.
1139 *Proceedings of the National Academy of Sciences* 112**,** E2829-E2835.
1140 Ebrahim, S.a.M., Dweck, H.K.M., Stökl, J., Hofferberth, J.E., Trona, F., Weniger, K.,
1141 Rybak, J., Seki, Y., Stensmyr, M.C., Sachse, S., Hansson, B.S., and Knaden, M.

(2015). *Drosophila* Avoids Parasitoids by Sensing Their Semiochemicals via a Dedicated Olfactory Circuit. *PLoS Biol* 13, e1002318.

Eckstein, N., Bates, A.S., Du, M., Hartenstein, V., Jefferis, G.S.X.E., and Funke, J. (2020). Neurotransmitter Classification from Electron Microscopy Images at Synaptic Sites in Drosophila. *bioRxiv*, 2020.2006.2012.148775.

Eichler, K., Litwin-Kumar, A., Li, F., Park, Y., Andrade, I., Schneider-Mizell, C.M., Saumweber, T., Huser, A., Eschbach, C., Gerber, B., Fetter, R.D., Truman, J.W., Priebe, C.E., Abbott, L.F., Thum, A.S., Zlatic, M., and Cardona, A. (2017). The Complete Connectome Of A Learning And Memory Center In An Insect Brain. *bioRxiv*.

Felsenberg, J., Jacob, P.F., Walker, T., Barnstedt, O., Edmondson-Stait, A.J., Pleijzier, M.W., Otto, N., Schlegel, P., Sharifi, N., Perisse, E., Smith, C.S., Lauritzen, J.S., Costa, M., Jefferis, G.S.X.E., Bock, D.D., and Waddell, S. (2018). Integration of Parallel Opposing Memories Underlies Memory Extinction. *Cell* 175, 709-722.e715.

Fiala, A. (2007). Olfaction and olfactory learning in Drosophila: recent progress. *Curr Opin Neurobiol* 17, 720-726.

Fishilevich, E., and Vosshall, L.B. (2005). Genetic and functional subdivision of the *Drosophila* antennal lobe. *Current biology* 15, 1548-1553.

Fröhlich, A. (1985). Freeze-Fracture Study of an Invertebrate Multiple-Contact Synapse: The Fly Photoreceptor Tetrad. *Journal of Comparative Neurology* 241, 311-326.

Galizia, C.G. (2014). Olfactory coding in the insect brain: data and conjectures. *European Journal of Neuroscience* 39, n/a-n/a.

Galizia, C.G., Nagler, K., Holldobler, B., and Menzel, R. (1998). Odour coding is bilaterally symmetrical in the antennal lobes of honeybees (Apis mellifera). *European Journal of Neuroscience* 10, 2964-2974.

Gao, Q., Yuan, B., and Chess, A. (2000). Convergent projections of Drosophila olfactory neurons to specific glomeruli in the antennal lobe. *Nature*.

Gao, X.J., Clandinin, T.R., and Luo, L. (2015). Extremely Sparse Olfactory Inputs Are Sufficient to Mediate Innate Aversion in *Drosophila PLoS ONE* 10, e0125986.

Gaudry, Q., Hong, E.J., Kain, J., De Bivort, B.L., and Wilson, R.I. (2013). Asymmetric neurotransmitter release enables rapid odour lateralization in *Drosophila*. *Nature* 493, 424-428.

Gondré-Lewis, M.C., Park, J.J., and Loh, Y.P. (2012). "Chapter Two - Cellular Mechanisms for the Biogenesis and Transport of Synaptic and Dense-Core Vesicles," in *International Review of Cell and Molecular Biology,* ed. K.W. Jeon. Academic Press), 27-115.

Goyal, R.K., and Chaudhury, A. (2013). Structure activity relationship of synaptic and junctional neurotransmission. *Autonomic Neuroscience: Basic and Clinical* 176, 11-31.

1183 Grabe, V., Baschwitz, A., Dweck, Hany k.M., Lavista-Llanos, S., Hansson, Bill s., and
1184 Sachse, S. (2016). Elucidating the Neuronal Architecture of Olfactory
1185 Glomeruli in the *Drosophila* Antennal Lobe. *Cell Reports* 16, 3401-3413.
1186 Grabe, V., and Sachse, S. (2018). Fundamental principles of the olfactory code.
1187 *Biosystems* 164, 94-101.
1188 Grabe, V., Schubert, M., Strube-Bloss, M., Reinert, A., Trautheim, S., Lavista-Llanos,
1189 S., Fiala, A., Hansson, B.S., and Sachse, S. (2020). Odor-Induced Multi-Level
1190 Inhibitory Maps in Drosophila. *eNeuro* 7.
1191 Grabe, V., Strutz, A., Baschwitz, A., Hansson, B.S., and Sachse, S. (2015). Digital in
1192 vivo 3D atlas of the antennal lobe of *Drosophila melanogaster*. *Journal of*
1193 *Comparative Neurology* 523, 530-544.
1194 Graubard, K., Raper, J.A., and Hartline, D.K. (1980). Graded synaptic transmission
1195 between spiking neurons. *Proc Natl Acad Sci U S A* 77, 3733-3735.
1196 Gruber, L., Rybak, J., Hansson, B.S., and Cantera, R. (2018). Synaptic Spinules in the
1197 Olfactory Circuit of Drosophila melanogaster. *Front Cell Neurosci* 12, 86.
1198 Guo, D., Wu, S., Chen, M., Perc, M., Zhang, Y., Ma, J., Cui, Y., Xu, P., Xia, Y., and
1199 Yao, D. (2016). Regulation of Irregular Neuronal Firing by Autaptic
1200 Transmission. *Sci Rep* 6, 26096.
1201 Guven-Ozkan, T., and Davis, R.L. (2014). Functional neuroanatomy of *Drosophila*
1202 olfactory memory formation. *Learning & Memory* 21, 519-526.
1203 Hallem, E.A., and Carlson, J.R. (2006). Coding of odors by a receptor repertoire. *Cell*
1204 125, 143-160.
1205 Hallem, E.A., Ho, M.G., and Carlson, J.R. (2004). The molecular basis of odor coding
1206 in the Drosophila antenna. *Cell* 117, 965-979.
1207 Hansson, B.S., and Anton, S. (2000). Function and morphology of the antennal lobe:
1208 new developments. *Annu Rev Entomol* 45, 203-231.
1209 Hartenstein, V. (2016). "The Central Nervous System of Invertebrates," in *The Wiley*
1210 *Handbook of Evolutionary Neuroscience,* ed. S.V. Shepherd.), 173-235.
1211 Haverkamp, A., Hansson, B.S., and Knaden, M. (2018). Combinatorial Codes and
1212 Labeled Lines: How Insects Use Olfactory Cues to Find and Judge Food,
1213 Mates, and Oviposition Sites in Complex Environments. *Front Physiol* 9, 49.
1214 Helmstaedter, M. (2013). Cellular-resolution connectomics: challenges of dense
1215 neural circuit reconstruction. *Nature Methods* 10, 501-507.
1216 Hirata, Y. (1964). Some observations on the fine structure of the synapses in the
1217 olfactory bulb of the mouse, with particular reference to the atypical synaptic
1218 configurations. *Archivum histologicum japonicum* 24, 293-302.
1219 Hong, E.J., and Wilson, R.I. (2015). Simultaneous encoding of odors by channels with
1220 diverse sensitivity to inhibition. *Neuron* 85, 573-589.
1221 Horne, J.A., Langille, C., Mclin, S., Wiederman, M., Lu, Z., Xu, C.S., Plaza, S.M.,
1222 Scheffer, L.K., Hess, H.F., and Meinertzhagen, I.A. (2018). A resource for the
1223 *Drosophila* antennal lobe provided by the connectome of glomerulus VA1v.
1224 *Elife* 7, e37550.

Huang, G.B., Scheffer, L.K., and Plaza, S.M. (2018). Fully-Automatic Synapse Prediction and Validation on a Large Data Set. *Frontiers in Neural Circuits* 12.

Hulse, B.K., Haberkern, H., Franconville, R., Turner-Evans, D.B., Takemura, S.-Y., Wolff, T., Noorman, M., Dreher, M., Dan, C., Parekh, R., Hermundstad, A.M., Rubin, G.M., and Jayaraman, V. (2021). A connectome of the Drosophila central complex reveals network motifs suitable for flexible navigation and context-dependent action selection. *eLife* 10**,** e66039.

Huoviala, P., Dolan, M.-J., Love, F.M., Myers, P., Frechter, S., Namiki, S., Pettersson, L., Roberts, R.J.V., Turnbull, R., Mitrevica, Z., Breads, P., Schlegel, P., Bates, A.S., Rodrigues, T., Aso, Y., Bock, D., Rubin, G.M., Stensmyr, M., Card, G., Costa, M., and Jefferis, G.S.X.E. (2020). Neural circuit basis of aversive odour processing in Drosophila from sensory input to descending output. 394403.

Ikeda, K., and Bekkers, J.M. Autapses. *Current Biology* 16**,** R308.

Ikeda, K., and Bekkers, J.M. (2006). Autapses. *Curr Biol* 16**,** R308.

Jeanne, James m., and Wilson, Rachel i. (2015). Convergence, Divergence, and Reconvergence in a Feedforward Network Improves Neural Speed and Accuracy. *Neuron* 88**,** 1014-1026.

Jefferis, G.S., Potter, C.J., Chan, A.M., Marin, E.C., Rohlfing, T., Maurer, C.R., Jr., and Luo, L. (2007). Comprehensive maps of *Drosophila* higher olfactory centers: spatially segregated fruit and pheromone representation. *Cell* 128**,** 1187-1203.

Karnovsky, M.J. (1965). A formaldehyde-glutaraldehyde fixative of high osmolarity for use in electron microscopy. *Journal of Cellular Biology* 27**,** 137.

Kazama, H., and Wilson, R.I. (2008). Homeostatic Matching and Nonlinear Amplification at Identified Central Synapses. *Neuron* 58**,** 401-413.

Kazama, H., and Wilson, R.I. (2009). Origins of correlated activity in an olfactory circuit. *Nat Neurosci* 12**,** 1136-1144.

Keene, A.C., and Waddell, S. (2007). Drosophila olfactory memory: single genes to complex neural circuits. *Nat Rev Neurosci* 8**,** 341-354.

Keesey, I.W., and Hansson, B.S. (2021). "10 - The neuroethology of labeled lines in insect olfactory systems," in *Insect Pheromone Biochemistry and Molecular Biology (Second Edition),* eds. G.J. Blomquist & R.G. Vogt. (London: Academic Press), 285-327.

Keesey, I.W., Zhang, J., Depetris-Chauvin, A., Obiero, G.F., Knaden, M., and Hansson, B.S. (2019). Evolution of a pest: towards the complete neuroethology of Drosophila suzukii and the subgenus Sophophora. *bioRxiv*, 717322.

Knaden, M., and Hansson, B.S. (2014). Mapping odor valence in the brain of flies and mice. *Curr Opin Neurobiol* 24**,** 34-38.

Knaden, M., Strutz, A., Ahsan, J., Sachse, S., and Hansson, B.S. (2012). Spatial representation of odorant valence in an insect brain. *Cell Reports* 1**,** 392-399.

1266 Knott, G., Marchman, H., and Lich, B. (2008). Serial Section Scanning Electron
1267 Microscopy of Adult Brain Tissue Using Focused Ion Beam Milling. *Journal of*
1268 *Neuroscience* 28, 2964-2959.
1269 Kreher, S.A., Mathew, D., Kim, J., and Carlson, J.R. (2008). Translation of sensory
1270 input into behavioral output via an olfactory system. *Neuron* 59, 110-124.
1271 Kumar, A., Schiff, O., Barkai, E., Mel, B.W., Poleg-Polsky, A., and Schiller, J. (2018).
1272 NMDA spikes mediate amplification of inputs in the rat piriform cortex. *eLife*
1273 7, e38446.
1274 Kurtovic, A., Widmer, A., and Dickson, B.J. (2007). A single class of olfactory
1275 neurons mediates behavioural responses to a Drosophila sex pheromone.
1276 *Nature* 446, 542-546.
1277 Laissue, P.P., Reiter, C., Hiesinger, P.R., Halter, S., Fischbach, K.F., and Stocker, R.F.
1278 (1999). Three-dimensional reconstruction of the antennal lobe in *Drosophila*
1279 *melanogaster*. *The Journal of Comparative Neurology* 405, 543-552.
1280 Laissue, P.P., and Vosshall, L.B. (2008). "The Olfactory Sensory Map in *Drosophila*," in
1281 *Brain Development in Drosophila melanogaster,* ed. G.M. Technau. (New York:
1282 Springer), 102-114
1283 Lei, H., Oland, L.A., Riffell, J.A., Beyerlein, A., and Hildebrand, J.G. (2010).
1284 "Microcircuits for Olfactory Information Processing in the Antennal Lobe of
1285 *Manduca sexta*," in *Handbook of Brain Microcircuits,* eds. G.M. Shepherd & S.
1286 Grillner. (New York: Oxford University Press), 417-426.
1287 Li, F., Lindsey, J.W., Marin, E.C., Otto, N., Dreher, M., Dempsey, G., Stark, I., Bates,
1288 A.S., Pleijzier, M.W., Schlegel, P., Nern, A., Takemura, S.Y., Eckstein, N.,
1289 Yang, T., Francis, A., Braun, A., Parekh, R., Costa, M., Scheffer, L.K., Aso, Y.,
1290 Jefferis, G.S., Abbott, L.F., Litwin-Kumar, A., Waddell, S., and Rubin, G.M.
1291 (2020a). The connectome of the adult Drosophila mushroom body provides
1292 insights into function. *Elife* 9.
1293 Li, H., Horns, F., Wu, B., Xie, Q., Li, J., Li, T., Luginbuhl, D.J., Quake, S.R., and Luo,
1294 L. (2017). Classifying Drosophila Olfactory Projection Neuron Subtypes by
1295 Single-Cell RNA Sequencing. *Cell* 171, 1206-1220.e1222.
1296 Li, P.H., Lindsey, L.F., Januszewski, M., Zheng, Z., Bates, A.S., Taisz, I., Tyka, M.,
1297 Nichols, M., Li, F., Perlman, E., Maitin-Shepard, J., Blakely, T., Leavitt, L.,
1298 Jefferis, G.S.X.E., Bock, D., and Jain, V. (2020b). Automated Reconstruction of
1299 a Serial-Section EM *Drosophila* Brain with Flood-Filling Networks and Local
1300 Realignment. *bioRxiv*, 605634.
1301 Liang, L., and Luo, L. (2010). The olfactory circuit of the fruit fly *Drosophila*
1302 *melanogaster*. *Sci China Life Sci* 53, 472-484.
1303 Lin, S., Kao, C.-F., Yu, H.-H., Huang, Y., and Lee, T. (2012). Lineage analysis of
1304 Drosophila lateral antennal lobe neurons reveals notch-dependent binary
1305 temporal fate decisions. *PLoS biology* 10, e1001425-e1001425.
1306 Liu, T.X., Davoudian, P.A., Lizbinski, K.M., and Jeanne, J.M. (2022). Connectomic
1307 features underlying diverse synaptic connection strengths and subcellular
1308 computation. *Current Biology* 32, 559-569.e555.

Liu, W.W., and Wilson, R.I. (2013). Glutamate is an inhibitory neurotransmitter in the *Drosophila* olfactory system. *Proceedings of the National Academy of Sciences* 110, 10294–10299.

Malun, D. (1991). Inventory and distribution of synapses of identified uniglomerular projection neurons in the antennal lobe of Periplaneta americana. *Journal of comparative neurology* 305, 348-360.

Malun, D., Waldow, U., Kraus, D., and Boeckh, J. (1993). Connections between the Deutocerebrum and the Protocerebrum, and Neuroanatomy of Several Classes of Deutocerebral Projection Neurons in the Brain of Male Periplaneta-Americana. *Journal of Comparative Neurology* 329, 143-162.

Marin, E.C., Büld, L., Theiss, M., Sarkissian, T., Roberts, R.J.V., Turnbull, R., Tamimi, I.F.M., Pleijzier, M.W., Laursen, W.J., Drummond, N., Schlegel, P., Bates, A.S., Li, F., Landgraf, M., Costa, M., Bock, D.D., Garrity, P.A., and Jefferis, G. (2020). Connectomics Analysis Reveals First-, Second-, and Third-Order Thermosensory and Hygrosensory Neurons in the Adult Drosophila Brain. *Curr Biol* 30, 3167-3182.e3164.

Masse, N.Y., Turner, G.C., and Jefferis, G.S. (2009). Olfactory information processing in Drosophila. *Curr Biol* 19, R700-713.

Masson, C., and Mustaparta, H. (1990). Chemical information processing in the olfactory system of insects. *Physiological Review* 70(1), 199-245.

Mctavish, T., Migliore, M., Shepherd, G., and Hines, M. (2012). Mitral cell spike synchrony modulated by dendrodendritic synapse location. *Frontiers in Computational Neuroscience* 6.

Meinertzhagen, I.A. (2018). Of what use is connectomics? A personal perspective on the *Drosophila* connectome. *Journal of Experimental Biology* 221, jeb164954.

Meinertzhagen, I.A., and O'neil, S.D. (1991). Synaptic organization of columnar elements in the lamina of the wild type in Drosophila melanogaster. *Journal of Comparative Neurology* 305, 232-263.

Miroschnikow, A., Schlegel, P., Schoofs, A., Hueckesfeld, S., Li, F., Schneider-Mizell, C.M., Fetter, R.D., Truman, J.W., Cardona, A., and Pankratz, M.J. (2018). Convergence of monosynaptic and polysynaptic sensory paths onto common motor outputs in a Drosophila feeding connectome. *eLife* 7, e40247.

Mohamed, A.a.M., Hansson, B.S., and Sachse, S. (2019a). Third-Order Neurons in the Lateral Horn Enhance Bilateral Contrast of Odor Inputs Through Contralateral Inhibition in Drosophila. *Front Physiol* 10, 851.

Mohamed, A.a.M., Retzke, T., Das Chakraborty, S., Fabian, B., Hansson, B.S., Knaden, M., and Sachse, S. (2019b). Odor mixtures of opposing valence unveil inter-glomerular crosstalk in the Drosophila antennal lobe. *Nat Commun* 10, 1201.

Mosca, T.J., and Luo, L. (2014). Synaptic organization of the *Drosophila* antennal lobe and its regulation by the Teneurins. *elife* 3, e03726.

Münch, D., and Galizia, C.G. (2016). DoOR 2.0 - Comprehensive Mapping of Drosophila melanogaster Odorant Responses. *Scientific Reports* 6, 21841.

1352 Nässel, D.R., Enell, L.E., Santos, J.G., Wegener, C., and Johard, H.A. (2008). A large
1353 population of diverse neurons in the Drosophila central nervous system
1354 expresses short neuropeptide F, suggesting multiple distributed peptide
1355 functions. *BMC Neurosci* 9, 90.
1356 Nässel, D.R., and Homberg, U. (2006). Neuropeptides in interneurons of the insect
1357 brain. *Cell Tissue Res* 326, 1-24.
1358 Ng, M., Roorda, R.D., Lima, S.Q., Zemelman, B.V., Morcillo, P., and Miesenböck, G.
1359 (2002). Transmission of Olfactory Information between Three Populations of
1360 Neurons in the Antennal Lobe of the Fly. *Neuron* 36, 463-474.
1361 Norgate, M., Lee, E., Southon, A., Farlow, A., Batterham, P., Camakaris, J., and
1362 Burke, R. (2006). Essential Roles in Development and Pigmentation for the
1363 *Drosophila* Copper Transporter DmATP7. *Molecular Biology of the Cell* 17, 475-
1364 484.
1365 Okada, R., Awasaki, T., and Ito, K. (2009). Gamma-aminobutyric acid (GABA)-
1366 mediated neural connections in the *Drosophila* antennal lobe. *Journal of*
1367 *Comparative Neurology* 514, 74-91.
1368 Olsen, S.R., and Wilson, R.I. (2008). Lateral presynaptic inhibition mediates gain
1369 control in an olfactory circuit. *Nature* 452, 956-960.
1370 Otto, N., Pleijzier, M.W., Morgan, I.C., Edmondson-Stait, A.J., Heinz, K.J., Stark, I.,
1371 Dempsey, G., Ito, M., Kapoor, I., Hsu, J., Schlegel, P.M., Bates, A.S., Feng, L.,
1372 Costa, M., Ito, K., Bock, D.D., Rubin, G.M., Jefferis, G.S.X.E., and Waddell, S.
1373 (2020). Input Connectivity Reveals Additional Heterogeneity of Dopaminergic
1374 Reinforcement in Drosophila. *Current Biology* 30, 3200-3211.e3208.
1375 Owald, D., and Waddell, S. (2015). Olfactory learning skews mushroom body output
1376 pathways to steer behavioral choice in Drosophila. *Current Opinion in*
1377 *Neurobiology* 35, 178-184.
1378 Parthasarathy, K., and Bhalla, U.S. (2013). Laterality and symmetry in rat olfactory
1379 behavior and in physiology of olfactory input. *J Neurosci* 33, 5750-5760.
1380 Prokop, A., and Meinertzhagen, I.A. (2006). Development and structure of synaptic
1381 contacts in Drosophila. *Semin Cell Dev Biol* 17, 20-30.
1382 Ronchi, P., Mizzon, G., Machado, P., D'imprima, E., Best, B.T., Cassella, L.,
1383 Schnorrenberg, S., Montero, M.G., Jechlinger, M., Ephrussi, A., Leptin, M.,
1384 Mahamid, J., and Schwab, Y. (2021). High-precision targeting workflow for
1385 volume electron microscopy. *J Cell Biol* 220.
1386 Root, C.M., Masuyama, K., Green, D.S., Enell, L.E., Nassel, D.R., Lee, C.H., and
1387 Wang, J.W. (2008). A presynaptic gain control mechanism fine-tunes olfactory
1388 behavior. *Neuron* 59, 311-321.
1389 Rospars, J.-P., Grémiaux, A., Jarriault, D., Chaffiol, A., Monsempes, C., Deisig, N.,
1390 Anton, S., Lucas, P., and Martinez, D. (2014). Heterogeneity and Convergence
1391 of Olfactory First-Order Neurons Account for the High Speed and Sensitivity
1392 of Second-Order Neurons. *PLOS Computational Biology* 10, e1003975.

Rozenfeld, E., Lerner, H., and Parnas, M. (2019). Muscarinic Modulation of Antennal Lobe GABAergic Local Neurons Shapes Odor Coding and Behavior. *Cell Rep* 29, 3253-3265.e3254.

Rybak, J. (2013). "Exploring Brain Connectivity in Insect Model Systems of Learning and Memory," in *Invertebrate Learning and Memory,* eds. R. Menzel & P. Benjamin. (San Diego: Academic Press), 26-40.

Rybak, J. (2016). "Perspective-Brain atlases for studying neuronal circuitry in arthropods," in *Structure and Evolution of Invertebrate Nervous Systems,* eds. A. Schmidt-Rhaesa, S. Harzsch & G. Purschke. (New York: Oxford University Press).

Rybak, J., and Hansson, B.S. (2018). "Olfactory Microcircuits in *Drosophila Melanogaster*," in *Handbook of Brain Microcircuits,* eds. G.M. Shepherd & S. Grillner. 2nd ed (Oxford, UK: Oxford University Press), 361-367.

Rybak, J., Talarico, G., Ruiz, S., Arnold, C., Cantera, R., and Hansson, B.S. (2016). Synaptic circuitry of identified neurons in the antennal lobe of *Drosophila melanogaster*. *J Comp Neurol* 524, 1920-1956.

Saada, R., Miller, N., Hurwitz, I., and Susswein, A.J. (2009). Autaptic excitation elicits persistent activity and a plateau potential in a neuron of known behavioral function. *Curr Biol* 19, 479-484.

Saalfeld, S., Cardona, A., Hartenstein, V., and Tomančák, P. (2009). CATMAID: collaborative annotation toolkit for massive amounts of image data. *Bioinformatics* 25, 1984-1986.

Sachse, S., and Galizia, C.G. (2002). Role of inhibition for temporal and spatial odor representation in olfactory output neurons: a calcium imaging study. *Journal of neurophysiology* 87, 1106-1117.

Sachse, S., and Hansson, B.S. (2016). "Research spotlight: Olfactory coding in *Drosophila melanogaster*," in *Structure and Evolution of Invertebrate Nervous Systems,* eds. A. Schmidt-Rhaesa, S. Harzsch & G. Purschke. (Oxford: Oxford University Press), 640-645.

Sachse, S., and Manzini, I. (2021). Editorial for the special issue "Olfactory Coding and Circuitries". *Cell Tissue Res* 383, 1-6.

Scheffer, L.K., Xu, C.S., Januszewski, M., Lu, Z., Takemura, S.-Y., Hayworth, K.J., Huang, G.B., Shinomiya, K., Maitlin-Shepard, J., Berg, S., Clements, J., Hubbard, P.M., Katz, W.T., Umayam, L., Zhao, T., Ackerman, D., Blakely, T., Bogovic, J., Dolafi, T., Kainmueller, D., Kawase, T., Khairy, K.A., Leavitt, L., Li, P.H., Lindsey, L., Neubarth, N., Olbris, D.J., Otsuna, H., Trautman, E.T., Ito, M., Bates, A.S., Goldammer, J., Wolff, T., Svirskas, R., Schlegel, P., Neace, E., Knecht, C.J., Alvarado, C.X., Bailey, D.A., Ballinger, S., Borycz, J.A., Canino, B.S., Cheatham, N., Cook, M., Dreher, M., Duclos, O., Eubanks, B., Fairbanks, K., Finley, S., Forknall, N., Francis, A., Hopkins, G.P., Joyce, E.M., Kim, S., Kirk, N.A., Kovalyak, J., Lauchie, S.A., Lohff, A., Maldonado, C., Manley, E.A., Mclin, S., Mooney, C., Ndama, M., Ogundeyi, O., Okeoma, N., Ordish, C., Padilla, N., Patrick, C.M., Paterson, T., Phillips, E.E., Phillips, E.M.,

Rampally, N., Ribeiro, C., Robertson, M.K., Rymer, J.T., Ryan, S.M., Sammons, M., Scott, A.K., Scott, A.L., Shinomiya, A., Smith, C., Smith, K., Smith, N.L., Sobeski, M.A., Suleiman, A., Swift, J., Takemura, S., Talebi, I., Tarnogorska, D., Tenshaw, E., Tokhi, T., Walsh, J.J., Yang, T., Horne, J.A., Li, F., Parekh, R., Rivlin, P.K., Jayaraman, V., Costa, M., Jefferis, G.S.X.E., et al. (2020). A connectome and analysis of the adult Drosophila central brain. *eLife* 9, e57443.

Schlegel, P., Bates, A.S., Stürner, T., Jagannathan, S.R., Drummond, N., Hsu, J., Serratosa Capdevila, L., Javier, A., Marin, E.C., Barth-Maron, A., Tamimi, I.F.M., Li, F., Rubin, G.M., Plaza, S.M., Costa, M., and Jefferis, G.S.X.E. (2021). Information flow, cell types and stereotypy in a full olfactory connectome. *eLife* 10, e66018.

Schneider-Mizell, C.M., Gerhard, S., Longair, M., Kazimiers, T., Li, F., Zwart, M.F., Champion, A., Midgley, F.M., Fetter, R.D., Saalfeld, S., and Cardona, A. (2016). Quantitative neuroanatomy for connectomics in *Drosophila*. *eLife* 5, e12059.

Seki, Y., Dweck, H.K.M., Rybak, J., Wicher, D., Sachse, S., and Hansson, B.S. (2017). Olfactory coding from the periphery to higher brain centers in the Drosophila brain. *BMC Biol* 15, 56.

Seki, Y., Rybak, J., Wicher, D., Sachse, S., and Hansson, B.S. (2010). Physiological and morphological characterization of local interneurons in the *Drosophila* antennal lobe. *Journal of Neurophysiology* 104, 1007-1019.

Semmelhack, J.L., and Wang, J.W. (2009). Select Drosophila glomeruli mediate innate olfactory attraction and aversion. *Nature* 459, 218-223.

Shanbhag, S.R., Muller, B., and Steinbrecht, R.A. (1999). Atlas of olfactory organs of *Drosophila melanogaster* - 1. Types, external organization, innervation and distribution of olfactory sensilla. *International Journal of Insect Morphology & Embryology* 28, 377-397.

Shepherd, G.M. (2011). "The Olfactory Bulb: A Simple System in the Mammalian Brain," in *Comprehensive Physiology*. John Wiley & Sons, Inc.).

Shepherd, G.M., Rowe, T.B., and Greer, C.A. (2021). An Evolutionary Microcircuit Approach to the Neural Basis of High Dimensional Sensory Processing in Olfaction. *Frontiers in Cellular Neuroscience* 15.

Silbering, A.F., and Galizia, C.G. (2007). Processing of odor mixtures in the Drosophila antennal lobe reveals both global inhibition and glomerulus-specific interactions. *J Neurosci* 27, 11966-11977.

Silbering, A.F., Okada, R., Ito, K., and Galizia, C.G. (2008). Olfactory information processing in the *Drosophila* antennal lobe: anything goes? *Journal of Neuroscience* 28, 13075-13087.

Silbering, A.F., Rytz, R., Grosjean, Y., Abuin, L., Ramdya, P., Jefferis, G.S., and Benton, R. (2011). Complementary Function and Integrated Wiring of the Evolutionarily Distinct *Drosophila* Olfactory Subsystems. *Journal of neuroscience* 31, 13357-13375.

Stensmyr, M.C., Dweck, H.K., Farhan, A., Ibba, I., Strutz, A., Mukunda, L., Linz, J., Grabe, V., Steck, K., Lavista-Llanos, S., Wicher, D., Sachse, S., Knaden, M., Becher, P.G., Seki, Y., and Hansson, B.S. (2012). A conserved dedicated olfactory circuit for detecting harmful microbes in *Drosophila*. *Cell* 151, 1345-1357.

Stocker, R.F., Lienhard, M.C., Borst, A., and Fischbach, K.F. (1990). Neuronal architecture of the antennal lobe in Drosophila melanogaster. *Cell and tissue research* 262, 9-34.

Stocker, R.F., Singh, R.N., Schorderet, M., and Siddiqi, O. (1983). Projection patterns of different types of antennal sensilla in the antennal glomeruli of Drosophila melanogaster. *Cell and Tissue Research* 232, 237-248.

Strutz, A., Soelter, J., Baschwitz, A., Farhan, A., Grabe, V., Rybak, J., Knaden, M., Schmuker, M., Hansson, B.S., and Sachse, S. (2014). Decoding odor quality and intensity in the *Drosophila* brain. *eLife* 3, e04147.

Su, C.-Y., Menuz, K., and Carlson, J.R. (2009). Olfactory Perception: Receptors, Cells, and Circuits. *Cell* 139, 45-59.

Suh, G.S.B., Wong, A.M., Hergarden, A.C., Wang, J.W., Simon, A.F., Benzer, S., Axel, R., and Anderson, D.J. (2004). A single population of olfactory sensory neurons mediates an innate avoidance behaviour in *Drosophila*. *Nature* 431, 854-859.

Sun, X.J., Tolbert, L.P., and Hildebrand, J.G. (1997). Synaptic organization of the uniglomerular projection neurons of the antennal lobe of the moth *Manduca sexta*: a laser scanning confocal and electron microscopic study. *Journal of Comparative Neurology* 379, 2-20.

Szyszka, P., and Galizia, C.G. (2015). "Olfaction in Insects," in *Handbook of Olfaction and Gustation,* ed. R.L. Doty. 3 ed: John Wiley & Sons, Inc), 531-546.

Taisz, I., Donà, E., Münch, D., Bailey, S.N., Morris, W.J., Meechan, K.I., Stevens, K.M., Varela, I., Gkantia, M., Schlegel, P., Ribeiro, C., Jefferis, G.S.X.E., and Galili, D.S. (2022). Generating parallel representations of position and identity in the olfactory system. *bioRxiv*, 2022.2005.2013.491877.

Takemura, S.-Y., Xu, C.S., Lu, Z., Rivlin, P.K., Parag, T., Olbris, D.J., Plaza, S., Zhao, T., Katz, W.T., Umayam, L., Weaver, C., Hess, H.F., Horne, J.A., Nunez-Iglesias, J., Aniceto, R., Chang, L.-A., Lauchie, S., Nasca, A., Ogundeyi, O., Sigmund, C., Takemura, S., Tran, J., Langille, C., Le Lacheur, K., Mclin, S., Shinomiya, A., Chklovskii, D.B., Meinertzhagen, I.A., and Scheffer, L.K. (2015). Synaptic circuits and their variations within different columns in the visual system of Drosophila. *Proceedings of the National Academy of Sciences* 112, 13711-13716.

Tamás, G., Buhl, E.H., and Somogyi, P. (1997). Massive Autaptic Self-Innervation of GABAergic Neurons in Cat Visual Cortex. *The Journal of Neuroscience* 17, 6352-6364.

Tanaka, N.K., Endo, K., and Ito, K. (2012). The organization of antennal lobe-associated neurons in the adult *Drosophila* melanogaster brain. *Journal of Comparative Neurology* 520, 4067-4130.

Thoma, M., Hansson, B.S., and Knaden, M. (2015). High-resolution Quantification of Odor-guided Behavior in Drosophila melanogaster Using the Flywalk Paradigm. *J Vis Exp*, e53394.

Tobin, W.F., Wilson, R.I., and Lee, W.-C.A. (2017). Wiring variations that enable and constrain neural computation in a sensory microcircuit. *eLife* 6, e24838.

Tran-Van-Minh, A., Cazé, R.D., Abrahamsson, T., Cathala, L., Gutkin, B.S., and Digregorio, D.A. (2015). Contribution of sublinear and supralinear dendritic integration to neuronal computations. *Frontiers in Cellular Neuroscience* 9.

Trujillo-Cenoz, O. (1969). Some Aspects of the Structural Organization of the Medulla in Muscoid Flies l. *J Ultrastructural Research* 27, 533-553.

Van Der Loos, H., and Glaser, E.M. (1972). Autapses in neocortex cerebri: synapses between a pyramidal cell's axon and its own dendrites. *Brain Res* 48, 355-360.

Vosshall, L.B., Wong, A.M., and Axel, R. (2000). An olfactory sensory map in the fly brain. *Cell* 102, 147-159.

Wang, J.W. (2012). Presynaptic modulation of early olfactory processing in *Drosophila*. *Developmental neurobiology* 72, 87-99.

Wicher, D., and Miazzi, F. (2021). Functional properties of insect olfactory receptors: ionotropic receptors and odorant receptors. *Cell Tissue Res* 383, 7-19.

Wiles, L., Gu, S., Pasqualetti, F., Parvesse, B., Gabrieli, D., Bassett, D.S., and Meaney, D.F. (2017). Autaptic Connections Shift Network Excitability and Bursting. *Sci Rep* 7, 44006.

Wilson, R.I. (2013). Early Olfactory Processing in Drosophila: Mechanisms and Principles. *Annual review of neuroscience* 36, 217-241.

Xu, C.S., Hayworth, K.J., Lu, Z., Grob, P., Hassan, A.M., García-Cerdán, J.G., Niyogi, K.K., Nogales, E., Weinberg, R.J., and Hess, H.F. (2017). Enhanced FIB-SEM systems for large-volume 3D imaging. *eLife* 6, e25916.

Xu, C.S., Januszewski, M., Lu, Z., Takemura, S.-Y., Hayworth, K.J., Huang, G., Shinomiya, K., Maitin-Shepard, J., Ackerman, D., Berg, S., Blakely, T., Bogovic, J., Clements, J., Dolafi, T., Hubbard, P., Kainmueller, D., Katz, W., Kawase, T., Khairy, K.A., Leavitt, L., Li, P.H., Lindsey, L., Neubarth, N., Olbris, D.J., Otsuna, H., Troutman, E.T., Umayam, L., Zhao, T., Ito, M., Goldammer, J., Wolff, T., Svirskas, R., Schlegel, P., Neace, E.R., Knecht, C.J., Alvarado, C.X., Bailey, D.A., Ballinger, S., Borycz, J.A., Canino, B.S., Cheatham, N., Cook, M., Dreher, M., Duclos, O., Eubanks, B., Fairbanks, K., Finley, S., Forknall, N., Francis, A., Hopkins, G.P., Joyce, E.M., Kim, S., Kirk, N.A., Kovalyak, J., Lauchie, S.A., Lohff, A., Maldonado, C., Manley, E.A., Mclin, S., Mooney, C., Ndama, M., Ogundeyi, O., Okeoma, N., Ordish, C., Padilla, N., Patrick, C., Paterson, T., Phillips, E.E., Phillips, E.M., Rampally, N., Ribeiro, C., Robertson, M.K., Rymer, J.T., Ryan, S.M., Sammons, M., Scott, A.K., Scott, A.L., Shinomiya, A., Smith, C., Smith, K., Smith, N.L., Sobeski,

M.A., Suleiman, A., Swift, J., Takemura, S., Talebi, I., Tarnogorska, D., Tenshaw, E., Tokhi, T., Walsh, J.J., Yang, T., Horne, J.A., Li, F., Parekh, R., Rivlin, P.K., Jayaraman, V., Ito, K., Saalfeld, S., George, R., Meinertzhagen, I., et al. (2020). A Connectome of the Adult *Drosophila* Central Brain. 2020.2001.2021.911859.

Yang, K., Liu, T., Wang, Z., Liu, J., Shen, Y., Pan, X., Wen, R., Xie, H., Ruan, Z., Tan, Z., Chen, Y., Guo, A., Liu, H., Han, H., Di, Z., and Zhang, K. (2022). Classifying Drosophila olfactory projection neuron boutons by quantitative analysis of electron microscopic reconstruction. *iScience* 25**,** 104180.

Yasuyama, K., Meinertzhagen, I.A., and Schurmann, F.W. (2003). Synaptic connections of cholinergic antennal lobe relay neurons innervating the lateral horn neuropile in the brain of *Drosophila melanogaster*. *J Comp Neurol* 466**,** 299-315.

Yasuyama, K., and Salvaterra, P.M. (1999). Localization of choline acetyltransferase-expressing neurons in *Drosophila* nervous system. *Microscopy Research and Technique* 45**,** 65-79.

Yin, L., Zheng, R., Ke, W., He, Q., Zhang, Y., Li, J., Wang, B., Mi, Z., Long, Y.-S., Rasch, M.J., Li, T., Luan, G., and Shu, Y. (2018). Autapses enhance bursting and coincidence detection in neocortical pyramidal cells. *Nature Communications* 9**,** 4890.

Yokoi, M., Mori, K., and Nakanishi, S. (1995). Refinement of odor molecule tuning by dendrodendritic synaptic inhibition in the olfactory bulb. *Proceedings of the National Academy of Sciences* 92**,** 3371-3375.

Zheng, Z., Lauritzen, J.S., Perlman, E., Robinson, C.G., Nichols, M., Milkie, D., Torrens, O., Price, J., Fisher, C.B., Sharifi, N., Calle-Schuler, S.A., Kmecova, L., Ali, I.J., Karsh, B., Trautman, E.T., Bogovic, J., Hanslovsky, P., Jefferis, G.S.X.E., Kazhdan, M., Khairy, K., Saalfeld, S., Fetter, R.D., and Bock, D.D. (2017). A Complete Electron Microscopy Volume Of The Brain Of Adult Drosophila melanogaster. *bioRxiv*.

Zheng, Z., Lauritzen, J.S., Perlman, E., Robinson, C.G., Nichols, M., Milkie, D., Torrens, O., Price, J., Fisher, C.B., Sharifi, N., Calle-Schuler, S.A., Kmecova, L., Ali, I.J., Karsh, B., Trautman, E.T., Bogovic, J.A., Hanslovsky, P., Jefferis, G.S.X.E., Kazhdan, M., Khairy, K., Saalfeld, S., Fetter, R.D., and Bock, D.D. (2018). A Complete Electron Microscopy Volume of the Brain of Adult Drosophila melanogaster. *Cell* 174**,** 730-743.e722.

1598 **FIGURES**

1599 **Figure 1: A correlative approach to analyze the ultrastructure of identified olfactory**
1600 **glomeruli**
1601 **A-B:** Two-photon laser scans of the antennal lobes in *Orco-Gal4; UAS-GCaMP6s* flies where
1602 Orco-positive olfactory sensory neurons (OSNs) in the glomerular neuropils were labeled
1603 by GCaMP (green fluorescence). Glomeruli DA2 (A) and DL5 (B) are encircled. Schematics
1604 show their relative position in the antennal lobe. Once the glomeruli of interest were
1605 identified, glomerular borders were marked with fiducial marks (arrowheads) via laser
1606 branding, which enabled their identification at the ultrastructural level. **C-D**:
1607 Representative images of the same glomeruli (DA2 in **C** and DL5 in **D**) obtained with
1608 focused-ion-beam electron microscopy (FIB-SEM), showing their ultrastructure. Asterisks
1609 indicate the main neurite of uniglomerular projection neurons entering the glomerulus.
1610 White arrowhead shows a 2-photon laser mark (see also **A** and **B**). **E**: FIB-SEM image of a
1611 polyadic synapse: the presynaptic site (red arrowhead) is composed of a T-bar shaped
1612 presynaptic density surrounded by small vesicles and is opposed by several postsynaptic
1613 profiles (cyan dots). Scheme of a tetrad synapse: a presynaptic site with its T-bar (red
1614 arrowhead) forms four output connections (arrows) with four postsynaptic input sites
1615 (cyan dots). **F:** A skeleton-based reconstruction of an OSN axon terminal (green line) with
1616 presynaptic (red dots) and postsynaptic sites (cyan dots). The dark grey shading
1617 surrounding the OSN trace represents the volume-based reconstruction of the same
1618 neuron. Tracing and reconstruction were performed within the FIB-SEM dataset (light grey
1619 area).
1620

1621 **Figure 2: Neuron classification and neuronal composition of the DA2 and DL5 glomeruli**
1622 **A**: Example FIB-SEM images (left column), volumetric neuronal reconstructions (middle
1623 column), and skeleton-based neuron traces (right column) of a representative example of
1624 each neuron class: OSNs (green), uniglomerular projection neurons (uPNs, red) and
1625 multiglomerular neurons (MGNs, blue). The ultrastructure of neurons, including T-bars
1626 (black arrowheads), mitochondria (asterisks) and spinules (white arrowhead) are
1627 indicated. Exemplar volumetric reconstructions (middle column) show the general
1628 morphology of each neuron class. Presynapses and postsynapses are indicated with red
1629 and cyan dots on the skeleton traces (right column). **B:** Average branching intensity
1630 (branching points per μm of neuronal-fiber length) of each neuron class OSNs, uPNs and
1631 MGNs in DA2 and DL5. Data represent mean+ standard deviation (error bars). Data points
1632 represent single values. Means were compared using Wilcoxon two-sample test. No
1633 significant differences of branching points/μm in OSNs or MGNs between glomeruli were
1634 found (significance was not tested for uPNs due to the presence of a single uPN in DL5).
1635 **C**: Schematic summary indicating, for each glomerulus, its volume (in μm^3), the number of

neurons of each class (MGNs were not counted), the total fiber length of all neurons for each neuron class and the total number of single synaptic contacts for each glomerulus.

Table 1. Glomerular innervation and synaptic composition

Quantitative neuronal data comparing glomeruli DA2 and DL5, detailing glomerular innervation and synaptic properties for each neuronal class: OSNs (green), uPNs (red) and MGNs (blue) and the sum of all of them. **Row 1**: Total length of all neurons of each neuron class and total length for all neurons in each glomerulus. **Row 2-4**: Synaptic counts: input sites (inputs), output sites (outputs) and T-bars (T-bars). **Row 5**: Innervation density: total neuron length (μm; row 1)/glomerular volume (μm^3); glomerular volume: DA2=1500 μm^3 and DL5=2700 μm^3 (see Figure 1C). **Row 6-8**: Total synaptic density per unit of glomerular volume (μm^3): sum of all input sites (inputs), output sites (outputs) and T-bars of each neuron class or of all neurons/glomerular volume. **Row 9-11**: Average synaptic density along neuronal fibers (illustrated also in Figure 3 – supplement 1): number of inputs, outputs or T-bars/neuron length (μm). **Row 12-13:** Average synaptic ratios: the ratio of T-bars-to-inputs or outputs-to-inputs. **Row 14:** Polyadicity: the average number of postsynaptic sites at each T-bar in DA2 and DL5. The ratios in rows 12-14 were calculated based on synaptic counts normalized to neuron length (rows 9-11). The color shading highlights values that have a relative difference greater than 20% (see relative differences Table S1) between DA2 and DL5. Dark shades highlights values that are greater in DA2 than in DL5 (green (OSNs), red (uPNs), blue (MGNs)) and light colors highlight values that are less in DA2 than in DL5.

Figure 3: Innervation density and synaptic density in DA2 and DL5

A-E: The average glomerular innervation density of OSNs (**A**), uPNs (**B**), MGNs (**C**) and collectively of all glomerular neurons (**D**); the average synaptic density of input sites (inputs), output sites (outputs) and T-bars and the average polyadicity. Innervation density: length (μm) of each neuronal fiber normalized to one μm^3 of glomerular (glom.) volume. Synaptic density: number of input sites, output sites or T-bars of each neuronal fiber normalized to one μm^3 of glomerular volume. Polyadicity: average number of single output sites per T-bar in each neuronal fiber. Data for DA2 shown in dark colors and for DL5 in light colors. Number of neurons in DA2: OSNs (green) n= 44; uPNs (red) n= 7; MGNs (blue) n=180; all neurons n=231, in DL5: OSNs n=46; uPN n=1; MGNs n=221; all neurons n=268. Data represent mean + standard deviation (error bars). Data points represent single values. Means were compared using either Student's t-test (OSNs) or Wilcoxon two-sample test (MGNs and all neurons). uPNs were not compared, since the DL5 has only one. Significance value: $p>0.05$ (not significant, no star), $p\leq0.05$ (*), $p\leq0.01$ (**), $p\leq0.001$ (***). Values are provided at data availability; polyadicity values are listed in Table 1, row 14.

1676 **Figure 4: Lateralization of OSN terminals in the antennal lobe**
1677 **A**: Illustration of an ipsilateral (dark green) and a contralateral (light green) OSN with
1678 dendrites in the corresponding antennae and their axonal projections to the ipsilateral
1679 olfactory glomerulus in the antennal lobe (AL) (dashed rectangle). **B**: Exemplary skeleton
1680 traces of an ipsilateral (dark green) and a contralateral (light green) OSN terminal inside
1681 glomerulus DA2. The ipsilateral OSN axons reach the glomerulus via the ipsilateral
1682 antennal nerve (arrow down) and leave the glomerulus towards the AL commissure
1683 (arrow up) while OSN axons originating at the contralateral antenna reach the glomerulus
1684 via the AL commissure. Red dots: presynapses; blue dots: postsynapses. **C**: Boxplots
1685 showing the fraction of synaptic output to uPNs (in red), - to OSNs (in green) or - toMGNs
1686 (in blue), , for the ipsilateral OSNs (dark green boxplot) and contralateral OSNs (light
1687 green), respectively, in the DA2, DL5 and VA1v glomeruli (VA1v data obtained from
1688 Horne et al., 2018). **D**: Boxplots showing the fraction of synaptic input of the same
1689 ipsilateral and contralateral OSNs that they receive from OSNs and MGNs. Connection
1690 polarity is indicated by arrows in the schematic neuronal drawings on the left of each plot.
1691 Dots represent single values. Means were compared using either Student's T-test.
1692 Significance value: $p>0.05$ (not significant, no star)), $p\leq0.05$ (*), $p\leq0.01$ (**), $p\leq0.001$ (***).
1693 Mean and Median values are provided at data availability.
1694
1695 **Figure 5: Strength of synaptic connection between neuron classes in the circuitry of DA2,**
1696 **DL5 and VA1v.**
1697 **A:** Schematic representation of principal connection motifs between the neuron classes
1698 OSNs (green), uPNs (red) and MGNs (blue). The synaptic flow directed towards uPNs is a
1699 feedforward and that directed towards OSNs or from uPNs to MGNs defined as a feedback
1700 connection (arrows). **B-D**: Alluvial diagrams of the glomerular circuitry in DA2 (**B**), DL5
1701 (**C**) and VA1v (**D**). Each diagram shows the relative synaptic strength calculated as the
1702 proportion of 1:1 single synaptic contacts between each neuron class in relation to the total
1703 number of synaptic contacts in their respective glomerulus. The synaptic strength between
1704 each neuron class, given as percentage, is indicated by the thickness of the lines. The
1705 proportions (as percentage) of output (left side) or input (right side) are illustrated by
1706 colored rectangles to the left or right of each alluvial diagram. The total number of synaptic
1707 contacts is indicated below the diagrams. Percentages of the relative synaptic strength and
1708 synaptic counts are listed in the supplementary Table S1. **E:** Stacked bar charts depict
1709 output (E') and input (E'') fractions (given as percentages) of each neuron class: OSNs
1710 (green), uPNs (red), MGNs (blue), schematically illustrated next to the bar charts
1711 respectively, to each of the other neuron classes for glomeruli DA2, DL5 and VA1v.
1712 Fractions are color-coded according to the neuron class of the respective connecting
1713 partner.
1714
1715

1716 **Figure 6: Differences in connectivity strength in glomeruli DA2, DL5 and VA1v**
1717 **A**: Schematic representation of synaptic connection motifs (arrows) between OSNs (green),
1718 uPNs (red), and MGNs (blue) in glomeruli DA2, DL5 and VA1v. The number of neurons
1719 of each class or truncated neuronal fibers (in brackets) is noted in the corresponding circle.
1720 **B**: Schematics of connection motifs (left) that are jointly stronger or weaker in DA2 and
1721 VA1v than in DL5. The relative differences (as percentage) between DA2 and DL5 as well
1722 as VA1v and DL5 are illustrated as arrows up (stronger) or arrows down (weaker)
1723 according to their intensity (see legend at the bottom) from the perspective of the target
1724 glomerulus (defined in the table header). The values of relative differences are listed in the
1725 Table S2.
1726
1727 **Figure 7: Distribution of pre- and postsynaptic partners of autapses in the uPN dendrite**
1728 **of the DL5**
1729 **A**: Distribution of autaptic presynaptic (red dots) and postsynaptic sites (cyan dots)
1730 mapped in a dendrogram of the dendrite of the single uPN in glomerulus DL5. The basal
1731 root node (black dot) represents the entry site of the uPN dendrite into the glomerulus
1732 (closest point to its soma). Clustering of autaptic input sites along some branches are
1733 encircled. **B**: Simplified representation of the uPN's dendrogram illustrating the distinct
1734 strahler orders, at distal branches (1-4) and at basal branches (5-8); see legend on the right).
1735 **C**: Distribution of autaptic presynaptic (left) and postsynaptic input sites (right) along the
1736 dendrite, as proportions at each corresponding strahler order (color coded). Note that
1737 autaptic postsynaptic sites are located almost exclusively at the most distal dendritic
1738 branches. **D**: Dendrogram of the DL5-uPN showing the distribution of presynaptic sites
1739 (triangles) and postsynaptic sites (circles) of selected autapses (indicated by same color).
1740 Distant pairs of pre- and postsynapses (long geodesic distance) are indicated by numbers
1741 whereas closely attached synaptic sites (short geodesic distance) are encircled and labelled
1742 with letters. **E**: Schematic of the dendrogram illustrating the location of the presynaptic
1743 (red dot) and postsynaptic (cyan dot) sites of a single autapse, the geodesic distance
1744 between them, i.e. the distance along the dendrite (μm), and the number of branching
1745 points (orange dots) between the pre- and postsynaptic components of the same autapse.
1746 **F**: Number of autapses with distinct geodesic distances between their pre- and
1747 postsynapses (illustrated in E). **G**: Number of autapses with the number of branch points
1748 between their pre- and postsynapses counted along the uPN dendrite (illustrated in E).

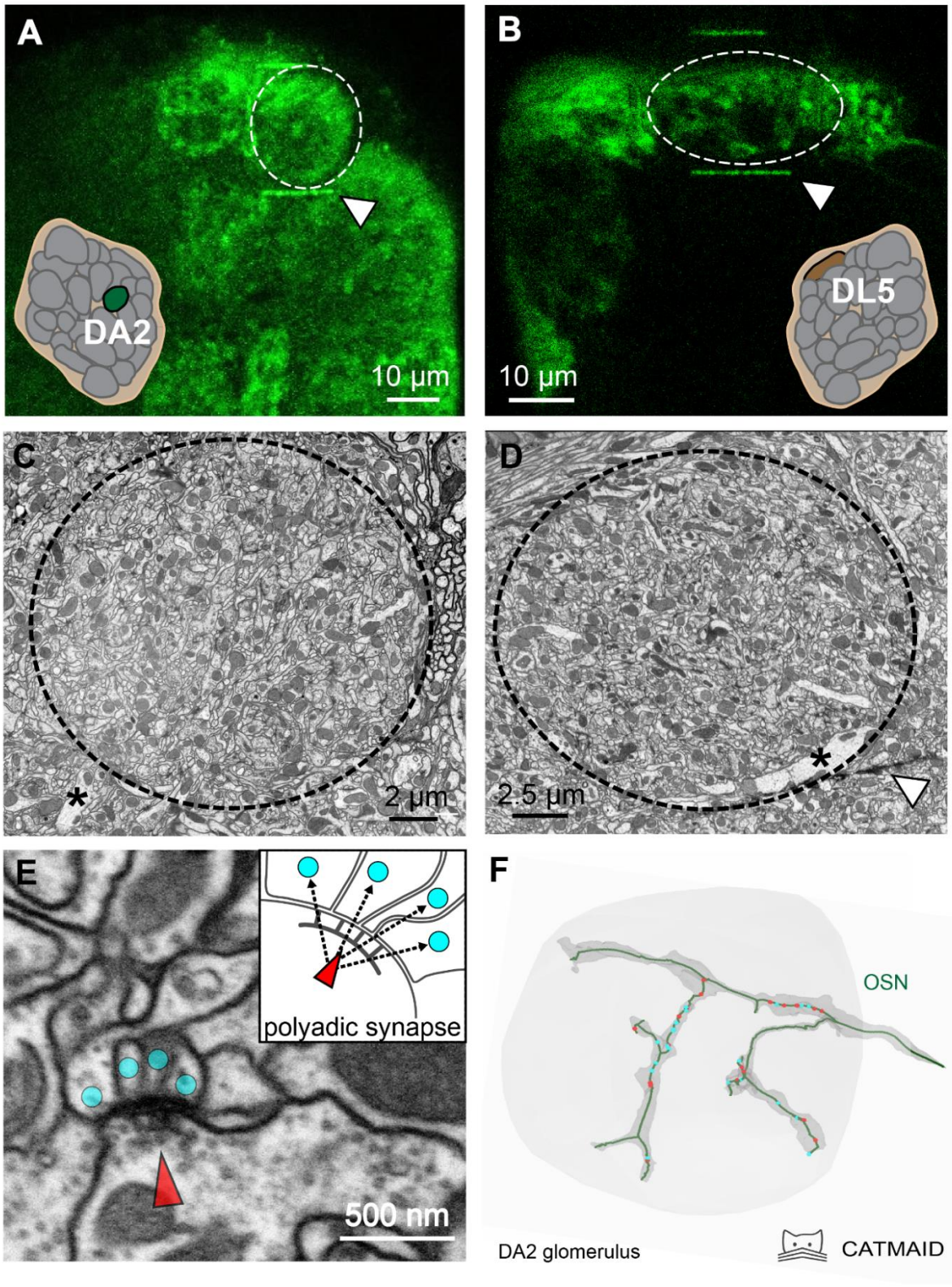
A
DA2
10 µm
B
DL5
10 µm
C
2 µm
D
2.5 µm
E
polyadic synapse
500 nm
F
OSN
DA2 glomerulus
CATMAID

Figure 1

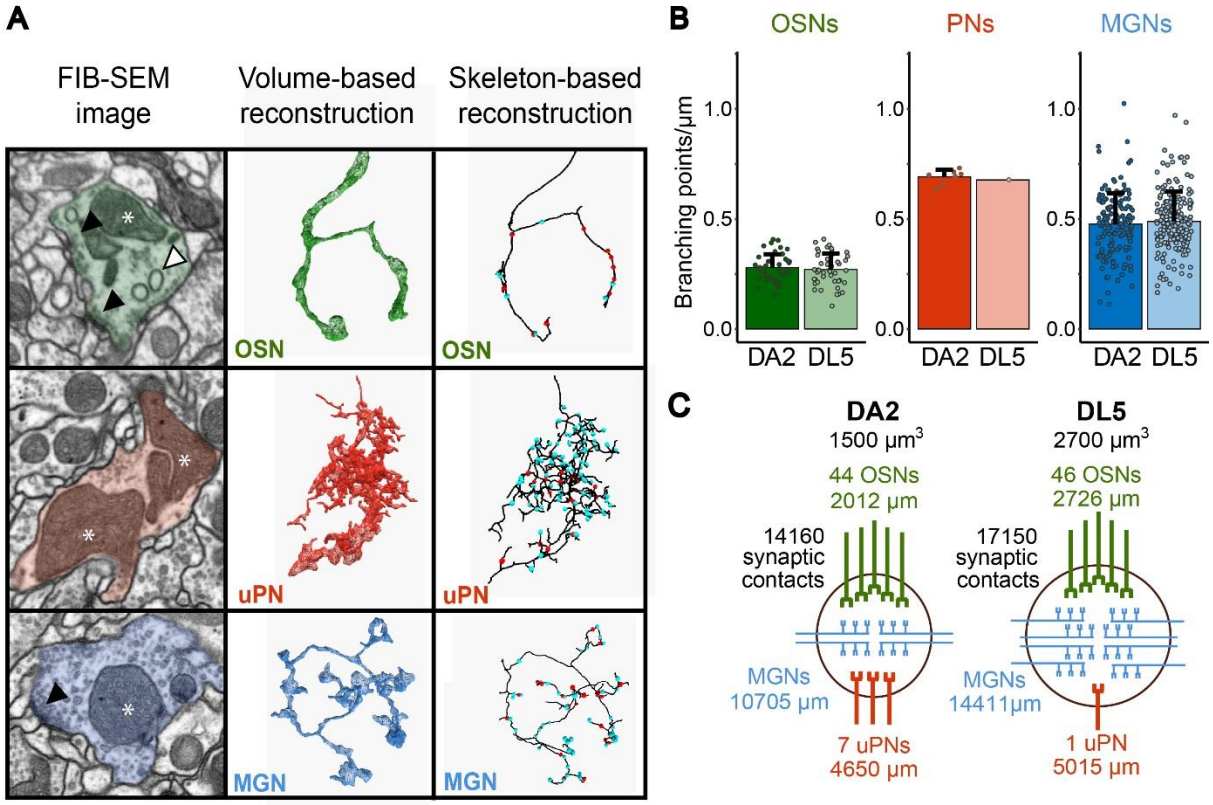
A
FIB-SEM image
Volume-based reconstruction
Skeleton-based reconstruction
OSN
OSN
uPN
uPN
MGN
MGN
B
OSNs
PNs
MGNs
Branching points/µm
1.0
0.5
0.0
DA2 DL5
C
DA2
1500 µm3
44 OSNs
2012 µm
14160 synaptic contacts
MGNs
10705 µm
7 uPNs
4650 µm
DL5
2700 µm3
46 OSNs
2726 µm
17150 synaptic contacts
MGNs
14411µm
1 uPN
5015 µm

Figure 2

Row	Values	Unit	OSNs		uPNs		MGNs		all neurons	
			DA2	DL5	DA2	DL5	DA2	DL5	DA2	DL5
1	**Total neuronal length**	µm	2012	2727	4652	5015	10705	14411	17370	22153
2	**Total synaptic counts**	input	868	1083	3887	3955	7229	9018	11984	14056
3		output	6671	6828	1624	3108	5659	6749	13954	16685
4		T-bars	1063	1213	322	602	1263	1572	2648	3387
5	**Total innervation density (sum of length of all neuronal fibers/glom. volume)**	µm/µm³	1.26	1.05	2.91	1.93	6.69	5.54	10.86	8.52
6	**Total glomerular synaptic density (total synaptic counts/glomerular volume)**	inputs/µm³	0.54	0.42	2.43	1.52	4.52	3.47	7.49	5.41
7		outputs/µm³	4.17	2.63	1.02	1.20	3.54	2.60	8.72	6.42
8		T-bars/µm³	0.66	0.47	0.20	0.23	0.79	0.60	1.66	1.30
9	**Neuronal synaptic density (synaptic counts/neuronal length)**	inputs/µm	0.42	0.39	0.83	0.79	0.62	0.59	0.59	0.56
10		outputs/µm	3.37	2.62	0.33	0.62	0.52	0.51	1.06	0.87
11		T-bars/µm	0.53	0.46	0.07	0.12	0.12	0.12	0.19	0.18
12	**Synaptic ratio**	T-bars/inputs	1.31	1.27	0.08	0.15	0.23	0.24	0.43	0.42
13		outputs/inputs	8.29	7.29	0.40	0.79	1.04	1.11	2.40	2.17
14	**Polyadicity**	outputs/T-bars	6.35	5.70	4.95	5.16	3.22	2.64	3.88	3.17

Table 1

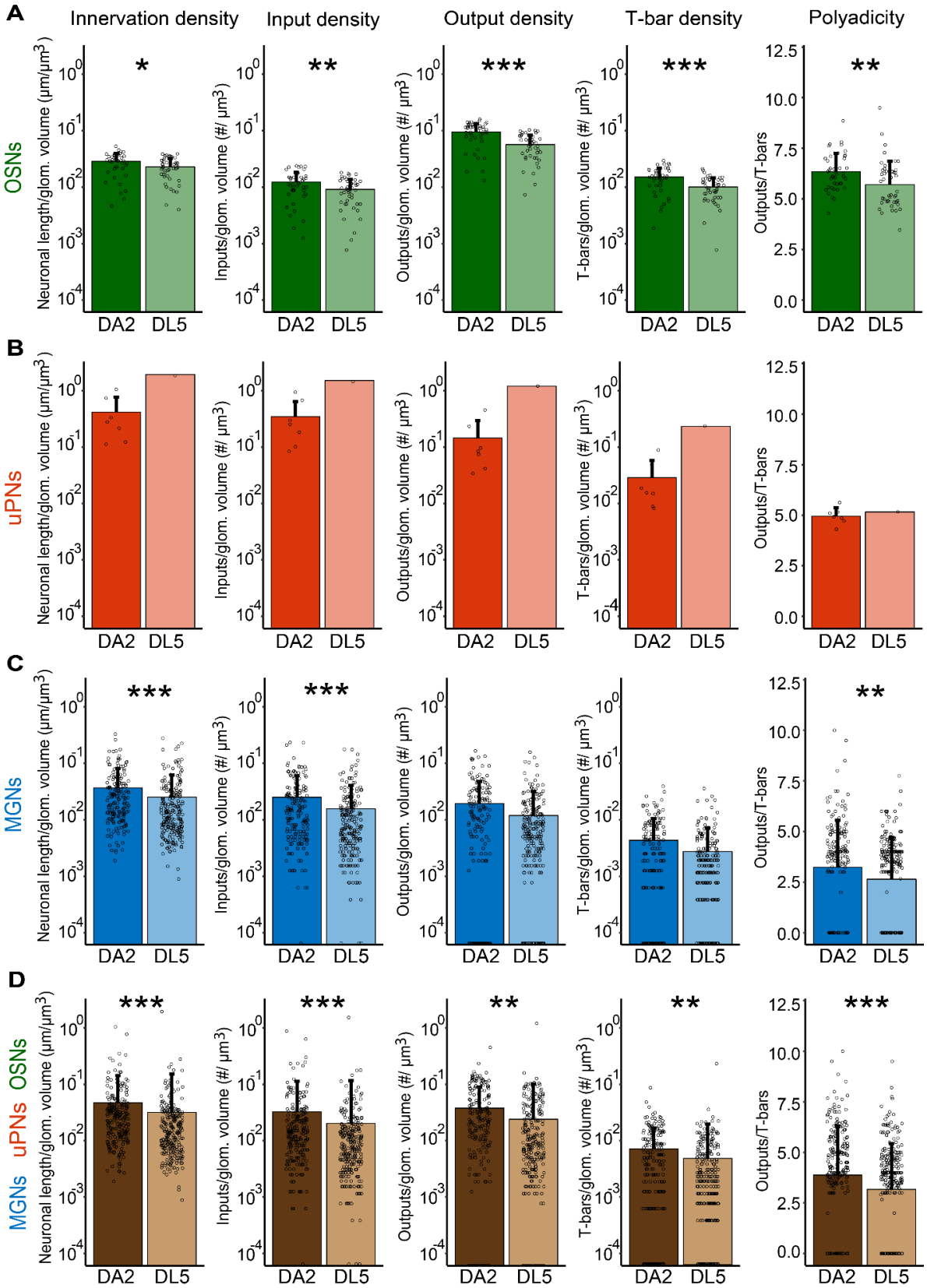
A
Innervation density
Input density
Output density
T-bar density
Polyadicity
OSNs
Neuronal length/glom. volume (µm/µm³)
Inputs/glom. volume (#/ µm³)
Outputs/glom. volume (#/ µm³)
T-bars/glom. volume (#/ µm³)
Outputs/T-bars
DA2
DL5
B
uPNs
C
MGNs
D
MGNs uPNs OSNs

Figure 3

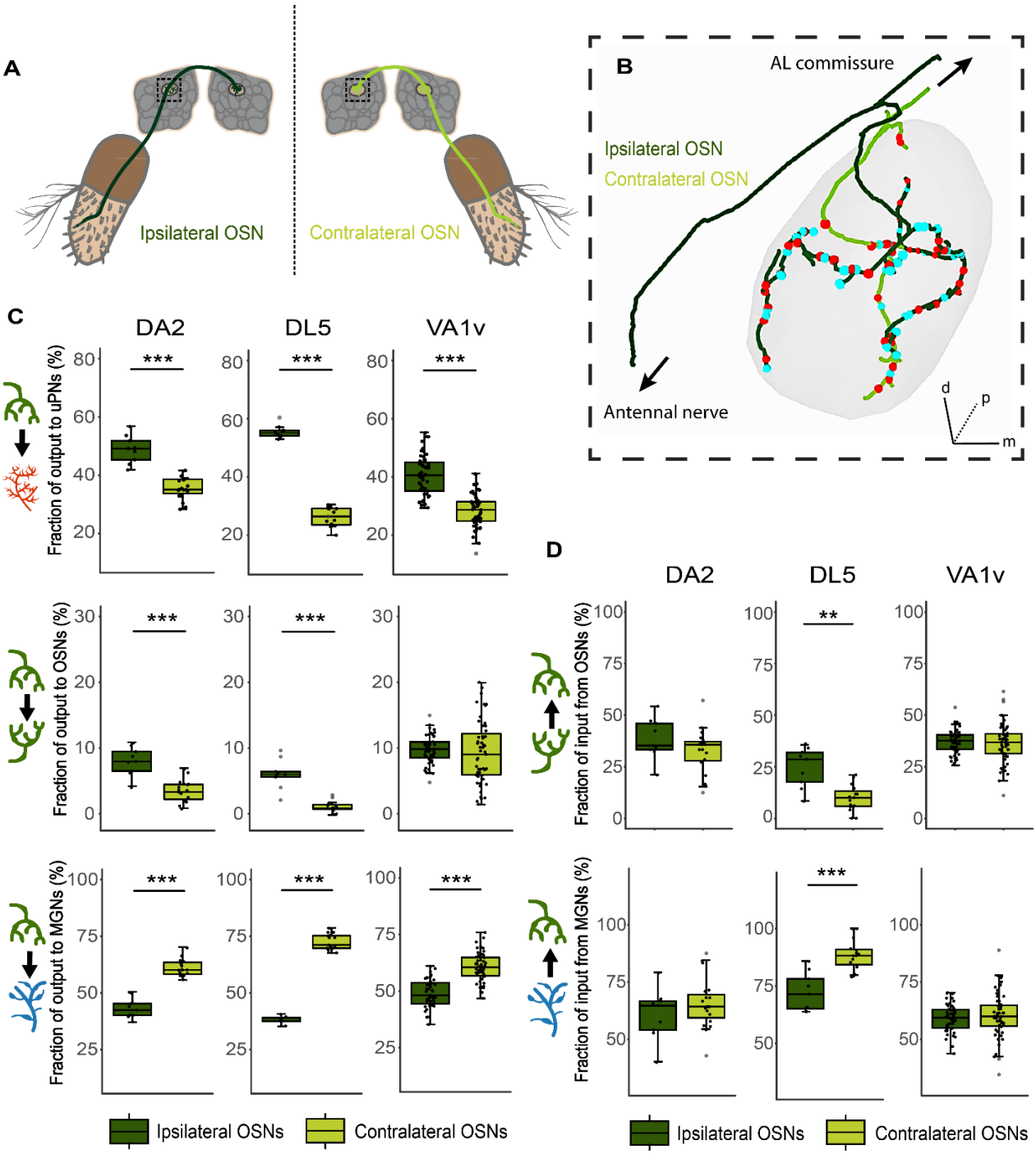
A
Ipsilateral OSN
Contralateral OSN
B
AL commissure
Ipsilateral OSN
Contralateral OSN
Antennal nerve
d
p
m
C
DA2
DL5
VA1v
Fraction of output to uPNs (%)
Fraction of output to OSNs (%)
Fraction of output to MGNs (%)
***
D
Fraction of input from OSNs (%)
Fraction of input from MGNs (%)
**
Ipsilateral OSNs
Contralateral OSNs

Figure 4

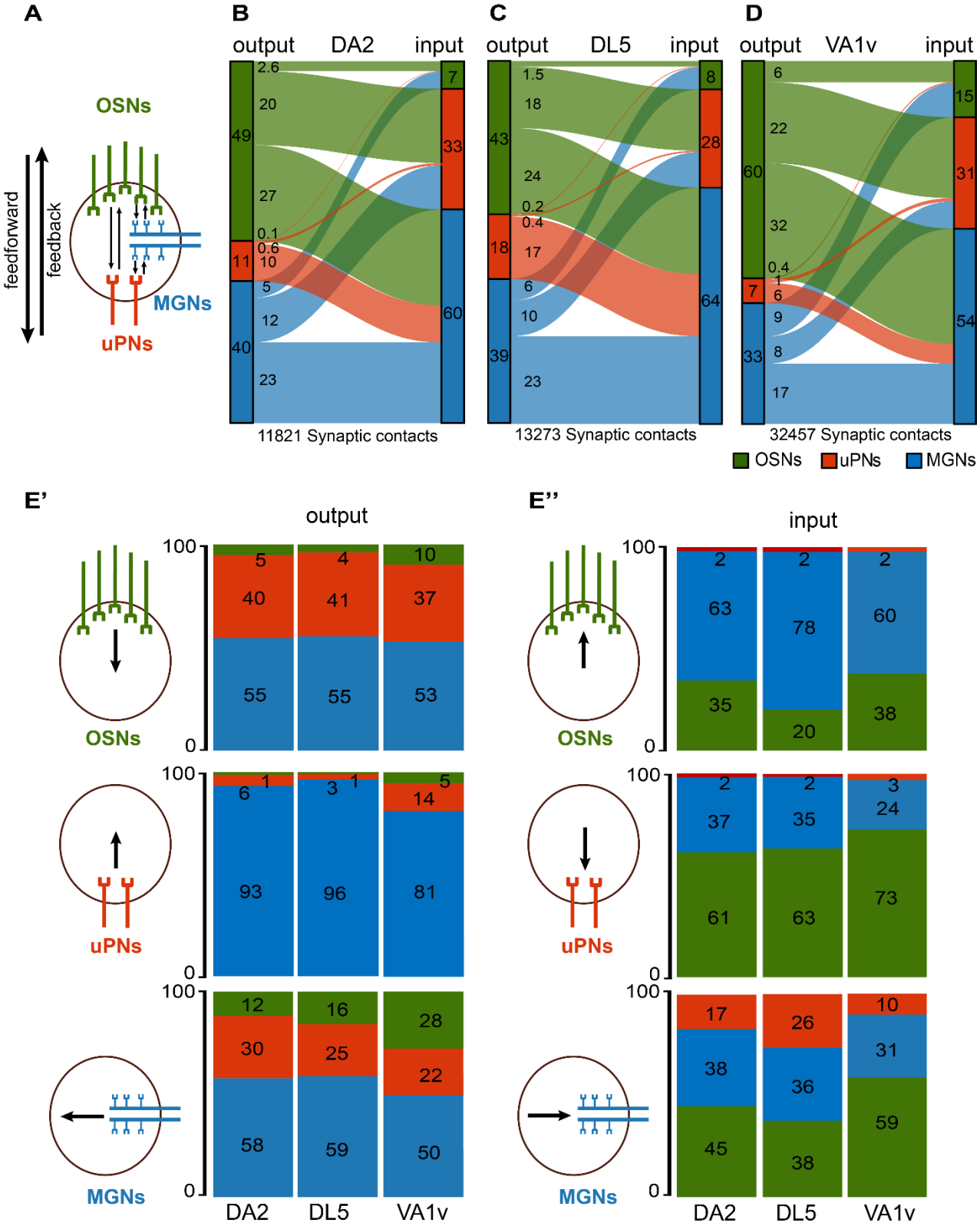
A
OSNs
feedforward
feedback
MGNs
uPNs
B
output
DA2
input
11821 Synaptic contacts
C
output
DL5
input
13273 Synaptic contacts
D
output
VA1v
input
32457 Synaptic contacts
OSNs
uPNs
MGNs
E'
output
E''
input
OSNs
uPNs
MGNs
DA2
DL5
VA1v

Figure 5

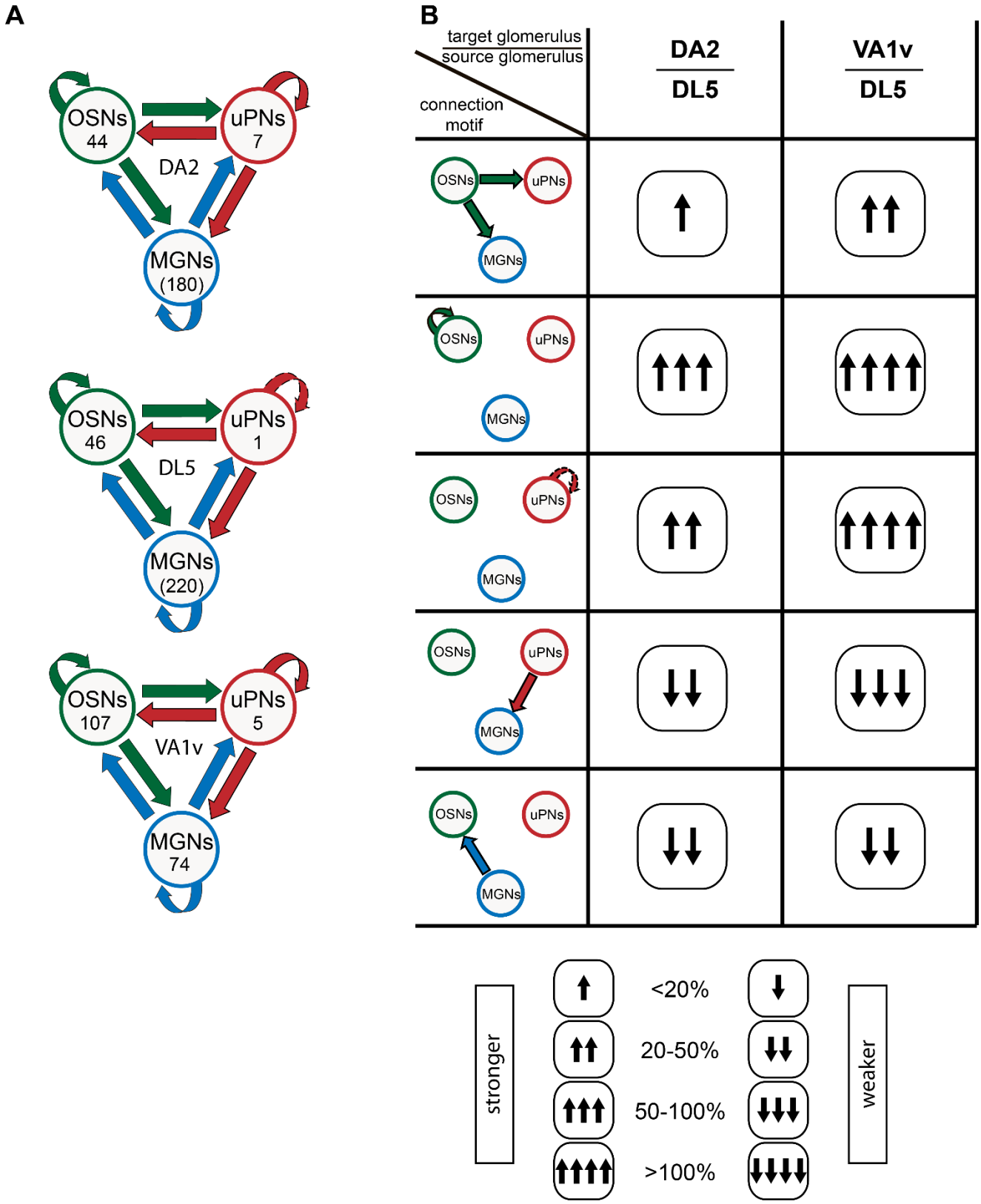
A
OSNs
44
uPNs
7
DA2
MGNs
(180)
OSNs
46
uPNs
1
DL5
MGNs
(220)
OSNs
107
uPNs
5
VA1v
MGNs
74
B
target glomerulus
source glomerulus
connection motif
DA2
DL5
VA1v
DL5
OSNs
uPNs
MGNs
stronger
<20%
20-50%
50-100%
>100%
weaker

Figure 6

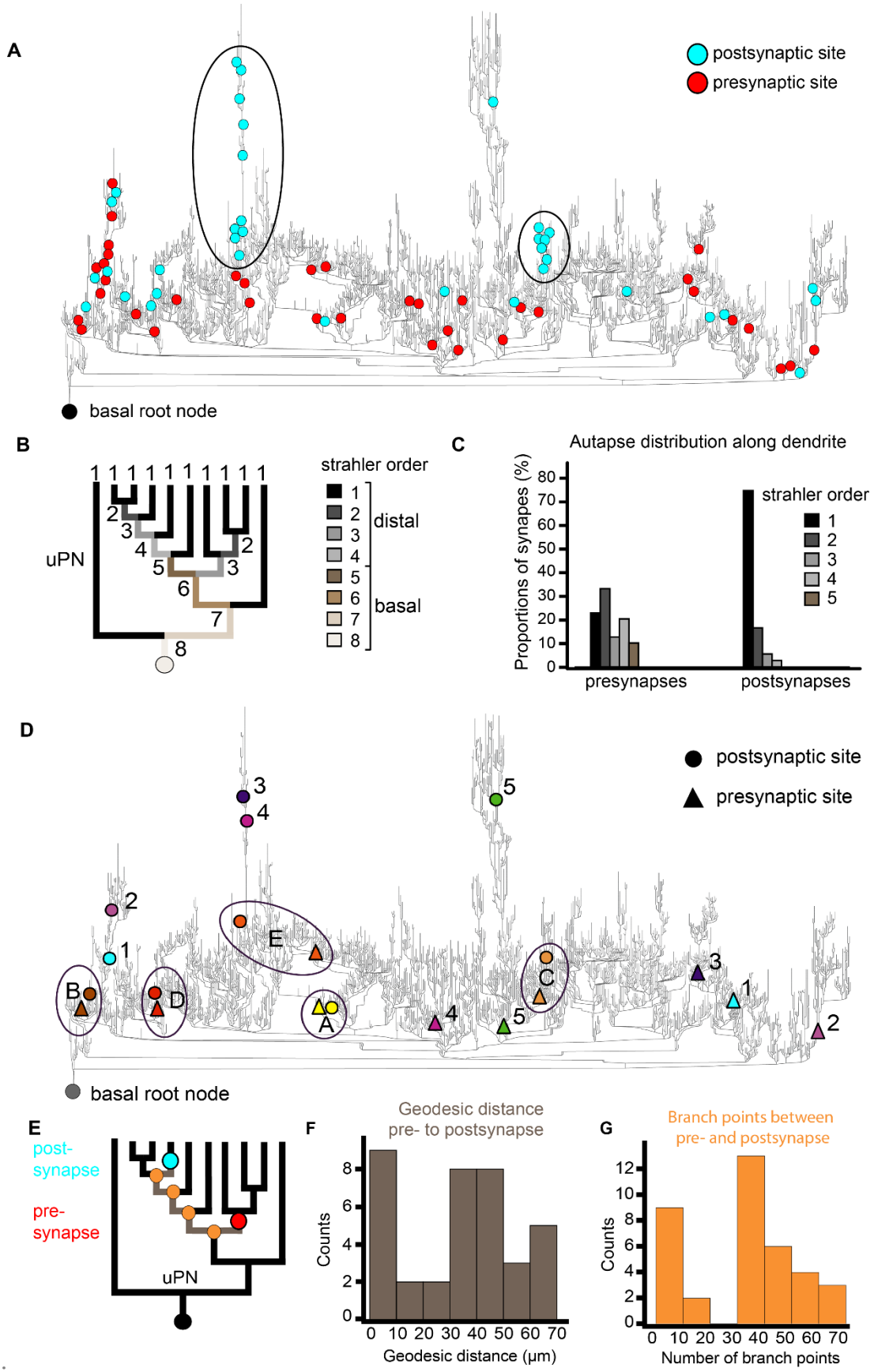
A
postsynaptic site
presynaptic site
basal root node
B
uPN
strahler order
distal
basal
C
Autapse distribution along dendrite
Proportions of synapses (%)
strahler order
presynapses
postsynapses
D
postsynaptic site
presynaptic site
basal root node
E
post-synapse
pre-synapse
uPN
F
Geodesic distance pre- to postsynapse
Counts
Geodesic distance (µm)
G
Branch points between pre- and postsynapse
Counts
Number of branch points

Figure 7